



POLITECNICO
MILANO 1863

SCUOLA DI INGEGNERIA INDUSTRIALE
E DELL'INFORMAZIONE

Analysis of the effects of the aortic conduit's geometry and mechanical behavior on heart valve prosthesis' test bench characterization

TESI DI LAUREA MAGISTRALE IN
MATERIALS ENGINEERING AND NANOTECHNOLOGY
BIOMEDICAL ENGINEERING
INGEGNERIA DEI MATERIALI E DELLE NANOTECNOLOGIE
INGEGNERIA BIOMEDICA

Author: Arianna Callera

Student ID: 944612

Advisor: Maria Laura Costantino, Roberto Frassine

Co-advisor: Marco Contino, Francesco De Gaetano, Stefano Tagliabue

Academic Year: 2021-22

Abstract

Any medical device, before reaching the market, has to follow a precise path: first pre-clinical trials that involve in vitro and in vivo test and then clinical trials. For cardiac valve prosthesis the information on the required procedures is contained in the ISO 5840:2021 in which is available the description of all the tests that need to be performed on a new prosthesis. In particular a pulsatile test is mandatory, however when describing its apparatus no indications are given on the characteristics of the tube downstream the aortic valve. As a result, this tube is often a straight, rigid conduit, not at all representative of the aorta.

This work concerns itself with modifying this conduit to introduce first the geometry, characterized by the Valsalva sinuses, and then the ascending aorta's compliance. In order to do this, a complete characterization is performed on a commercial polymeric material, the Elastic 50 A resin by Formlabs. In particular several tests were performed including a tensile test to find the elastic modulus and cyclic test to ensure survival to testing. The results obtained were used to 3D print the conduit with the correct geometry and compliance. Then, according to the Standard, pulsatile tests were performed on three heart valve prosthesis: a mechanical, a polymeric, and a biological one; in three configurations: standard, rigid with Valsalva sinuses and compliant with Valsalva sinuses.

With the complete characterization it was possible to obtain the aortic phantom and use it during testing. From said tests emerged that the introduction of the Valsalva sinuses led to a decrease in regurgitation, due to vortex formation. The compliance instead led to an increase in regurgitation due to backflow from the tube's pulsatile behaviour. The effect on the valves was also related to the type of prostheses tested.

From these results we can see how the lack of precise directions on the aortic downstream conduit in the Standard leaves everyone the freedom to test the valves in non-physiological conditions that cannot properly predict how the valve will perform in the human body.

Key-words: heart valve prosthesis, aortic phantom, standard, geometry, mechanical properties, 3D printing.

Abstract in italiano

Qualunque dispositivo medico, prima di raggiungere il mercato, deve seguire una precisa procedura: per prima cosa vanno effettuati dei test preclinici, in vitro e in vivo, e solo dopo i test clinici. Per le protesi di valvola cardiaca le procedure qui indicate sono esemplificate nella normativa ISO 5840. Nella norma viene prescritta l'esecuzione di un test pulsatile in condizioni fisiologiche, ma la descrizione dell'apparato da utilizzare manca di precise indicazioni sul condotto a valle della valvola aortica che risulta quindi in molti apparati essere un tubo rigido e dritto, per nulla rappresentativo dell'aorta.

Questo lavoro si è occupato di modificare il sopracitato condotto per introdurre prima la corretta geometria caratterizzata dai seni di Valsalva e poi la capacitanza dell'aorta ascendente. Per quest'ultima è stato necessario eseguire una completa caratterizzazione su un materiale polimerico, la resina elastic 50A della Formlabs, al fine di ottenere le proprietà ricercate. In particolare sono stati eseguiti svariati test, fra cui test a trazione per caratterizzare il modulo elastico e test ciclici per verificare che il tubo potesse sopportare i test. I risultati raccolti sono stati utilizzati per produrre un condotto cedevole e con la geometria dei seni di Valsalva realizzato tramite stampa 3D. Sono stati poi eseguiti test pulsatili secondo normativa su tre protesi diverse: meccanica, polimerica e biologica; nella configurazione standard, con un tubo rigido con geometria e poi con il tubo cedevole con geometria.

Grazie alla completa caratterizzazione eseguita sul materiale è stato così possibile realizzare il phantom aortico e utilizzarlo nei test. Da questi è risultato che l'introduzione dei seni di Valsalva porta a una riduzione del rigurgito valvolare, probabilmente dovuta alla formazione di vortici. L'introduzione della capacitanza ha condotto a un aumento del rigurgito dovuto a un contro flusso generato dalla pulsatilità del condotto.

Da questi risultati emerge come la mancanza nella normativa di indicazioni sul condotto a valle della valvola aortica lasci la libertà di eseguire i test in condizioni lontane da quelle fisiologiche e con risultati che non rispecchiano adeguatamente le prestazioni che la valvola avrà nel corpo umano.

Parole chiave: protesi valvolari cardiache, phantom aortico, normativa, geometria, proprietà meccaniche, stampa 3D.

Contents

Abstract	i
Abstract in italiano	iii
Contents	v
Introduction	1
Aim	1
Importance of physiological in vitro tests	1
Standard and planned improvements	2
1 Anatomy	3
1.1. An introduction of the cardiovascular system.....	3
1.2. The heart.....	4
1.2.1. Heart physiology.....	4
1.2.2. Heart valves	5
1.3. Ascending aorta.....	9
1.3.1. Geometry and mechanical properties	9
1.3.2. Role of Valsalva sinuses	9
1.3.3. Role of compliance	10
2 State of the art	13
2.1. Standard for heart valve prostheses testing	13
2.2. Test benches developed.....	14
2.2.1. Test benches on the market.....	14
2.2.2. Test benches developed by different researchers.....	15
2.2.3. Aortic models.....	17
3 Polymer characterization	19
3.1. Properties of the natural aorta.....	19
3.2. Materials and methods	20
3.2.1. Choice of resin	20
3.2.2. Sample production.....	20
3.2.3. Tests.....	21
3.3. Results.....	28
3.4. Final conduit design	44

4	Valve Testing	45
4.1.	Aim	45
4.2.	Materials and methods	45
4.2.1.	Description of test bench	45
4.2.2.	Pulsatile test	46
4.2.3.	Different types of conduits used	46
4.2.4.	Types of valve prosthesis tested.....	50
4.3.	Results	52
	Conclusion and future developments	69
	Bibliography	71
	List of Figures	75
	List if Tables	79
	List of symbols	81
	Glossary of Acronyms	83
	Acknowledgments	85

Introduction

Aim

Heart valve diseases are one of the most common diseases in the modern world. It is estimated that in 2020 more than 250000 heart valve surgeries were performed [1]. Replacement of a heart valve does not come without consequences and the prosthetic valves are far from perfect. In an attempt to improve patient outcome, in the last years we have assisted to the birth of several innovations in prosthesis types [2]: to the most common mechanical and biological heart valve prosthesis, polymeric ones are added while new techniques are studied to allow the implant of the valve without open heart surgery thanks to transcatheter valves.

With the increasing number of options arises the need for an effective comparison method that allows to predict which type of prosthesis will have the best in vivo behavior. In vitro testing is the first step for approval of a new prosthesis and could be suitable to perform an effective comparison between different valve types. However, the Standard in vitro test is very far from the physiological condition and may give results far away from the situation in the human body. This work focuses on introducing more physiological conditions for testing of aortic valve prosthesis and comparing the changes in behavior of different valve substitutes in these conditions.

Importance of physiological in vitro tests

The commercialization process for a new medical device involves a battery of in vitro tests that aim to check different characteristics of the device, in vivo tests with a close animal model and only at the end clinical trials. Animal tests are expensive, complicated to carry out and can never perfectly reproduce the condition in the human body; for all these reasons it would be better to reduce their role as much as possible and have them become a simple validation step. In order to do that it is necessary to improve the in vitro tests and bring them as close as possible to reality, this would allow to cut the costs, reduce ethical problems, and speed up the reach of the market allowing for a faster evolution of technologies. It would also likely lead to a general increase of success of clinical trials with evident benefits for the patients involved in it. Moreover, it is worth considering that a testing system that is too far away from the real situation may not reproduce some characteristics that could improve the performance of some devices and therefore lead to the exclusion of a system that would have well performed in a human body.

In this work we will focus on improving the aortic model inside a pulsatile test bench already present in our lab and on the effect that this will have on the performance of different aortic valve prosthesis. Since our goal is to derive general knowledge, we will use a parametric model derived from average physiological conditions rather than a patient specific one. In the future, realization of some patient specific aortic roots may be useful to select the most appropriate prosthesis in presence of some peculiar anatomy.

An appropriate aortic model should be realistic in terms of pressure/velocity characteristics and accurate in terms of mechanical and geometrical features of the vessel wall [3]. To satisfy these requirements we will reproduce as closely as possible the internal geometry and the compliance of the aorta.

Standard and planned improvements

Heart valve prosthesis are commonly tested according to the Standard ISO 5840. For surgically implanted valves the Standard calls, among others, for a hydrodynamic pulsatile test in which the nominal pulsatile-flow conditions should be fixed and physiological. While specifications are given on the compliance of chambers nothing is mentioned on tubes; as a result, straight, rigid tubes are used [4]. This particularly interesting if we consider the tube downstream the aortic housing that should represent the aorta. In this work we will first introduce the geometry of the Valsalva sinuses only and then add the aortic compliance; we expect the prosthesis to be affected by these changes and therefore to behave in a more similar way to what happens in vivo [5].

In order to design a conduit with the required compliance the first portion of this work will focus on the selection and characterization of a polymeric material. In order to be able to later obtain the complex geometry of the Valsalva sinuses the material was chosen from a catalogue of 3D printing resins already available on the market. The choice was done based on reported elongation and strength at break, trying to match the aorta's properties. The material then underwent a series of mechanical tests in order design a conduit with the appropriate mechanical behaviour and that would allow to perform all required tests.

1 Anatomy

1.1. An introduction of the cardiovascular system

The cardiovascular system is made up by the heart and the blood circulation system; the latter comprehends arteries, veins, and capillaries. The heart is divided into two non-communicating halves: the right and the left heart; each of them is divided into two communicating chambers: the atrium and the ventriculus. Arteries take the blood from the heart to the districts while veins take it back; the passage from arteries to veins happens trough capillaries where the oxygen and catabolites exchange with the tissues happens. Blood circulation is granted by the pumping action of the heart that pushes blood around the system; since the heart is a pulsatile pump the pressure in the vessels will not be constant. In particular, the higher-pressure variation is reached in the aorta between 80 and 120 mmHg. Throughout the system the pulsation effect is reduced by the compliance of the vessels. The vascular system can be divided into pulmonary and systemic circulation.

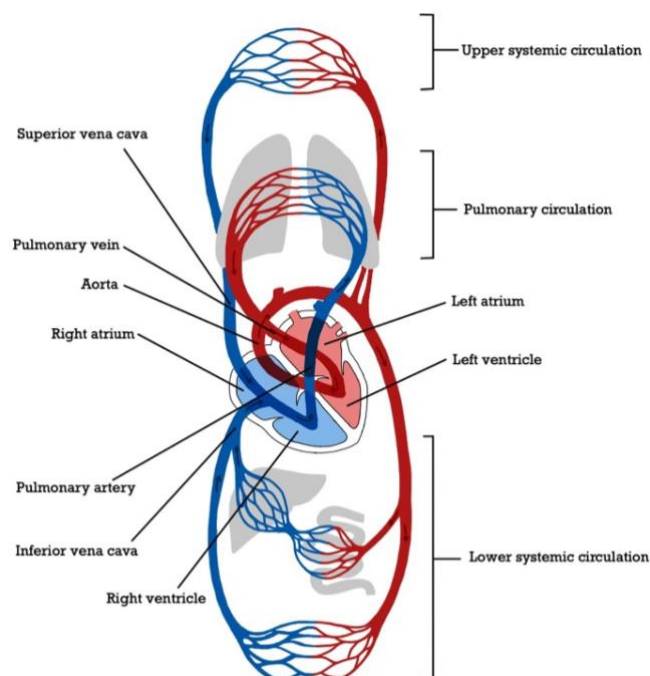


Figure 1.1: The cardiovascular system

The pulmonary circulation starts in the right atrium where blood is collected from the superior and inferior vena cava, from there it passes into the right ventricle and is then pushed into the pulmonary artery. This vessel takes the blood into the lungs and then the pulmonary vein carries the oxygenated blood to the left atrium.

The systemic circulation starts in the left atrium, from there blood passes to the left ventricle and is then pushed into the aorta. From different portions of the aorta arteries originate to bring blood to all districts. After the capillary exchange in the tissues blood is collected by veins that merge into the superior and inferior vena cava and bring it back to the right atrium to restart the cycle [6].

1.2. The heart

1.2.1. Heart physiology

As stated before, the heart has the fundamental role of pumping blood throughout the entire body; in order to do that it is equipped with a strong muscular structure and four non-returns, passive, valves; two between the atria and the ventricles (atrioventricular: tricuspid and mitral) and two between the ventricles and the arteries (semilunar: pulmonary and aortic). These valves ensure unidirectional flow of blood during the cardiac cycle. The cardiac cycle lasts on average 0.7-0.8 seconds and is characterized by four phases: isovolumetric contraction, ejection, isovolumetric relaxation, and filling. During the first phase the ventriculus contracts and its pressure increases provoking the closure of the atrioventricular valves, when the pressure is high enough the semilunar valves open and the ejection phase takes place pushing the blood in the aorta and the pulmonary trunk. Then isovolumetric relaxation of the ventricle happens and the pressure inside the ventricle decreases, because of this the semilunar valves close [6]. At this point the low pressure in the ventricle determines the opening of the atrioventricular valves, the ventricle is filled by blood and the cycle can start again. Since the left heart pumps blood to the whole body, it needs to generate higher pressures and is equipped with thicker walls.

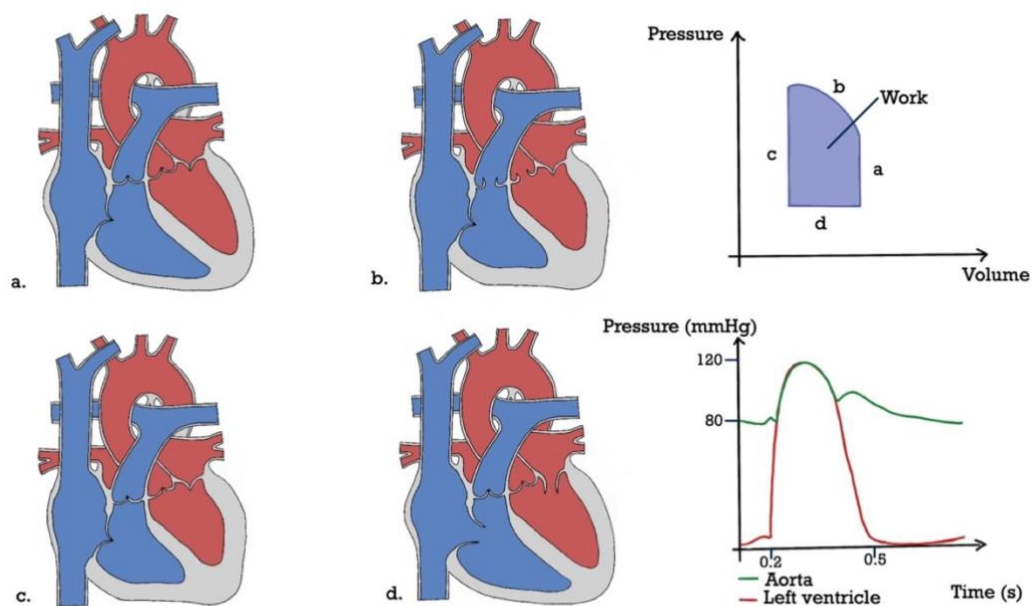


Figure 1.2: Phases of the cardiac cycle with drawings, pressure-volume graph, and pressure-time behavior

1.2.2. Heart valves

Structure and function

The correct opening and closure of the valves is fundamental to ensure efficient work of the heart; their movement is governed by the pressure difference between upstream and downstream chambers. The cardiac cycle is repeated at every heartbeat and the valves will open on average at least $3 \cdot 10^9$ times during a lifetime; it is then clear how strong and resistant these structures have to be to support us [7].

Atrioventricular valves are positioned between the atria and the ventriculi and they are composed by cusps: limbs of connective tissue connected at the base to the atrioventricular orifice and with the free end connected with by tendineae cords to papillae muscles. During contraction of the ventricle papillae muscles contract and the tendineae cords tend helping the closure and keeping in situ the cusps avoiding prolapse into the atrium. The left valve has two cusps while the right one has three.

Semilunar valves are positioned at the origin of the pulmonary trunk (right) and the aorta (left). Both valves are composed by three folds of connective tissue that block the backflow of blood into the ventricle. At valve level both on the aorta and on the pulmonary trunk there are dilatations called sinuses [6].

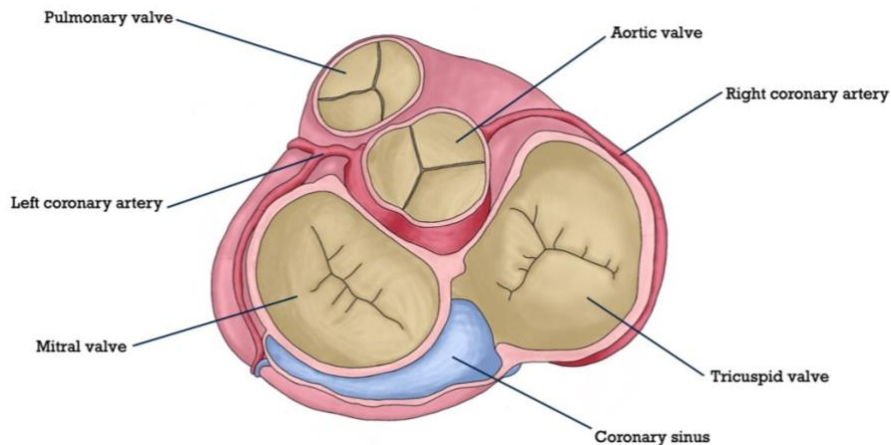


Figure 1.3: View of the valve plane with the four valves clearly visible

The extracellular matrix of heart valves is composed by three layers, each with a specific function. The fibrosa and the spongiosa are the same for both semilunar and atrioventricular; the third one is the ventricularis for the semilunar valves and the atrialis for the atrioventricular ones. The fibrosa is composed of circumferential collagen fibers and provides stiffness; atrialis and ventricularis are made of radial elastic fibers and are key to tissue motion; finally, the spongiosa is composed by proteoglycans and interspersed collagen fibers to ensure compressibility and tissue integrity [8].

The structure of each valve is slightly different, the aortic valve, on which this work is centered, is here described. The aortic valve is composed of three cusps: left coronary, right coronary, and non-coronary. The structure of the valve creates a self-contained support structure into the aortic root. The semilunar shape is given by the crown-shaped anulus.

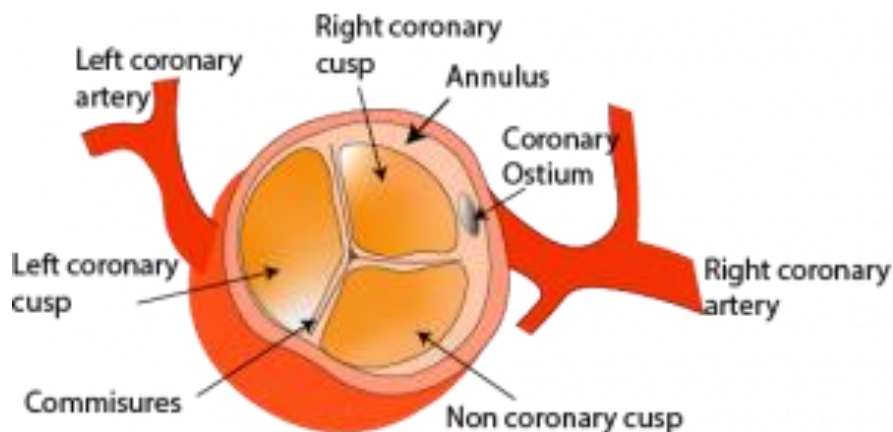


Figure 1.4: Anatomy of the aortic valve

Pathologies

Heart valves can be affected by congenital or acquired pathologies that are essentially classified into two categories: insufficiency and stenosis. A valve affected by insufficiency is not able to close properly and will result in a regurgitation of some blood volume with a consequent increase of work of the heart that has to compensate for the backflow. A valve affected by stenosis is not able to open completely and will result in an increase of work of the heart that has to pump against a higher resistance. In general, the left valves are more affected by pathologies since they are subjected to higher pressures; in particular, aortic valve stenosis is the most common valve disease. Valve diseases tend to progress and to this day no pharmacological treatment exists to reduce degeneration of heart valves, so the only possible treatment is surgery either to repair the valve, for example with clips, or to substitute it with a prosthetic one [2].

Types of heart valve prostheses

The ideal heart valve prosthesis should replicate the natural function perfectly, be durable, easy to implant, independent of anticoagulants and have no inherent pressure gradient [9]. These requirements are yet to be satisfied and currently three main categories of surgically implantable valves can be identified: mechanical, biological, and polymeric. To these we could add tissue engineered valves that will not be treated here since they are still under study.

Mechanical valves were the first attempt at a heart valve prosthesis; they are made of metallic, polymeric, or ceramic elements that are not deformed but move to allow the correct function. After many devices and many improvements currently the most used type is a bileaflet valve with leaflets covered in pyrolytic carbon, a durable and antithrombotic material, with a Dacron ring for sutures. This type of valves are very durable, they can function up to 30 years, but require continuous anticoagulant therapy and are therefore not applicable to some categories of patients like women in fertile age and people in countries without regular access to medication. Another disadvantage of these valves is that they alter the fluid dynamic of the system and, in case of rupture, there is no progressive damage leading to failure and therefore need more monitoring.



Figure 1.5: Bileaflet mechanical valve

Biological valves were introduced to overcome the need for anticoagulants, they can be made with either porcine valves or sutured bovine pericardium treated with glutaraldehyde generally mounted on metallic or polymeric structures to increase stability. Since these valves are based on deformable tissues their functioning is more similar to the physiological one compared to mechanical valves and their degradation is progressive and gives rise to cardiac symptoms. Despite being less thrombogenic these valves have low durability, around 10-15 years, and are therefore not advisable for younger patients that would require several reinterventions [10]. With the increase of life expectancy, the short life of a biological valve makes them problematic also for 60 years old patients that do not want to risk a following surgery at older age.



Figure 1.6: Stented biological valve

Polymeric heart valves are the most recent ones and have the goal of placing themselves in between the first two categories: overcome the need of anticoagulants like biological ones but have the same durability as mechanical ones. The polymers used include but are not limited to a styrene triblock copolymer [2] and a siloxane-based polyurethane-urea [11]. The latter, commercially called Lifepolymer, has shown great hemocompatibility, great resistance to degradation and good durability. Clinical trials have started in 2021 [11].

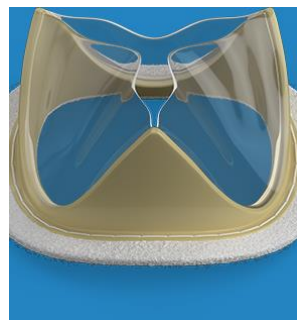


Figure 1.7: Tria heart valve, made with Lifepolymer by Foldax

It is worth mentioning that beside surgically implantable valves the new category of transcatheter valves is emerging with the goal of reducing the associated risks and allow the implant into more patients like elderly patients or those who cannot withstand an open-heart procedure. These valves are generally produced based on biological valves, but some prototypes of polymeric TAVI are under study.

1.3. Ascending aorta

1.3.1. Geometry and mechanical properties

The aorta is the main artery that, from the left ventricle, brings oxygenated blood to the whole body, it is divided into three segments: ascending aorta, aortic arch, and descending aorta. Since the carried flow changes throughout its path, the vessel has different characteristics according to the observed area. Since we are focusing on the effect of the vessel's properties on the aortic valve the ascending aorta is studied in detail. It is the largest segment of the aorta, with a caliber of 2.8-3.0 cm, and the only arteries that originate from it are the coronary arteries in the right and left Valsalva sinuses.

The aorta, like all other arteries is characterized by a three-layer wall structure. The most internal layer, the intima, is made up by endothelial cells in basal direction on a basal membrane that sits on a subendothelial collagen layer; between the intima and the median layer there is the internal elastic membrane. The median layer is composed by elastic fibers, collagen, and proteoglycans; between the median layer and the outer layer there is the outer elastic membrane. The outer layer, the adventitia, is made up by connective tissue in the longitudinal direction; in this layer we find the nerves and the vasa vasorum, the circulation of the large blood vessels [6]. This structure makes the aorta a very elastic vessel able to accommodate the heart's pulsation.

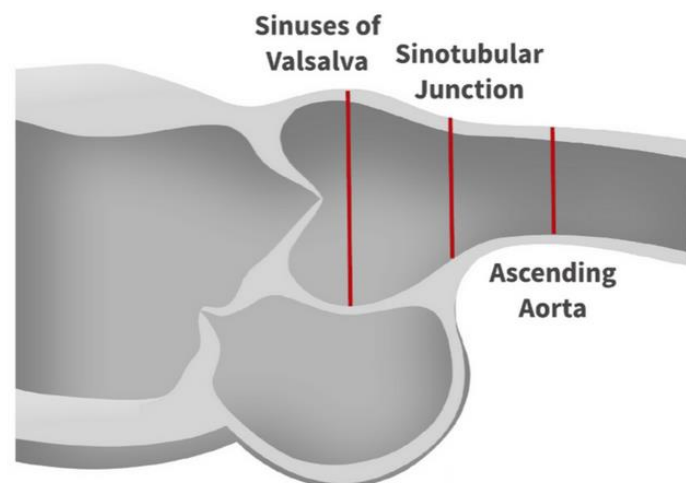


Figure 1.8: Structure of vessel downstream the aortic valve

1.3.2. Role of Valsalva sinuses

The most important geometrical characteristic that gets overlooked in the Standard is the presence of Valsalva sinuses at the aortic root. The Valsalva sinuses, or aortic sinuses, are an anatomical dilatation of the aorta just downstream the aortic valve

where the coronaries originate [12]. The presence of this sinuses has been correlated to the formation of some vortexes right downstream the valve towards the end of the systolic phase. This action is believed to push the aortic leaflets toward the center of the vessel and to facilitate the closure of the valve, even if the pressure difference alone would be enough to provoke the closure [7]. Since with the sinuses the closure is faster and easier it is reasonable to assume that their presence should reduce regurgitation. Some studies also suggest that the presence of the sinuses provokes the formation of startup vortexes during early systole helping the opening of the valve. Moreover, the presence of the sinuses allows more space for the leaflets' expansions allowing a better opening [13].

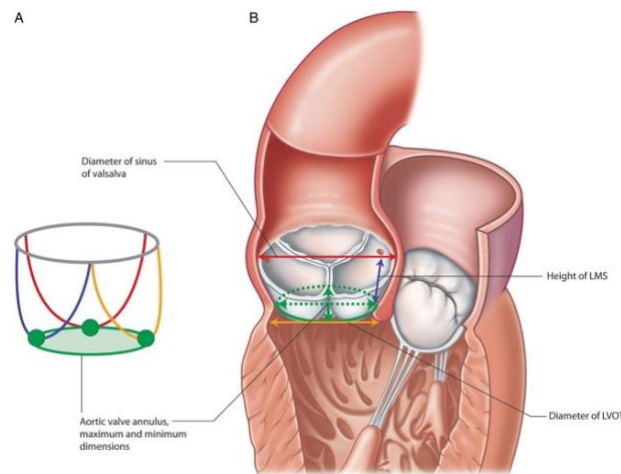


Figure 1.9: Anatomy of the aortic valve showing the enlargement of the Valsalva sinuses

From this analysis it is clear how not considering the sinuses is likely to alter the performance of valve prosthesis.

The exact measurements of the aorta are patient specific and strongly dependent on flow conditions. Because of this, when trying to describe precisely the Valsalva sinuses most several works focus on the relationship between the annulus and the maximum diameter at the sinuses [14].

1.3.3. Role of compliance

The second fundamental characteristic of a good aortic model is the correct compliance; as a matter of fact compliance is believed to be the main factor affecting the overall behavior of the model and in particular the magnitude of the strain field. In fact, if we consider the physiological role of the aorta its compliance is of cardinal importance to transform the pulsatile flow of the heart into a continuous flow to oxygenate all the organs. The aortic root is especially relevant if we consider coronary perfusion, since the coronaries originate in the Valsalva sinuses if the root was not compliant their perfusion could happen only during systole while with this characteristic the majority of perfusion happen in diastole thanks to arterial pressure. Especially since we are considering a pulsatile test the presence of a compliant vessel

will impact the fluid dynamics and pressures of the system. The goal is to have a system with a behavior analogous to the physiological one, so a system that will expand during systole and recoil during diastole.

In the years many studies have been performed to measure the aortic compliance, mainly with the objective to better understand the mechanism that leads to the formation of aneurisms. The techniques used are several but can be divided in two categories: mechanical testing performed of aortas harvested from cadavers or transesophageal echocardiography performed during routine exams. While the first allows to perform a more complete analysis, the second has the advantage of evaluating the performance of the vessel in vivo. Given the different techniques used and the fact that we are dealing with a human tissue, that has intrinsically variable mechanical properties, the results found in literature can be very inhomogeneous. After the literature review a value of $0.01 \text{ cm}^2/\text{mmHg}$ per unit length has been found in an echocardiographic study [15] and with a direct study in vivo [16].

2 State of the art

2.1. Standard for heart valve prostheses testing

Since many models of valves exist and more are coming out each year, it is fundamental to have a standardised set of tests that the product must overcome before reaching clinical trials. The European standard for cardiac valve prostheses is the EN ISO 5840 [4]; this Standard includes all the information related to: in vitro and in vivo tests, packaging, labeling and sterilization requirements. In particular, in the 2021 version, the standard is divided into three parts: the first one contains general information regarding all valves, the second is specifically for testing surgical valves while the last one is for transcatheter valves. The information contained in the following sections are derived from the ISO 5840-2. Between all the tests listed the one that replicates most closely the in vivo conditions is the hydrodynamic pulsatile performance assessment; for this reason, we will focus on that. Hydrodynamic tests should be performed in both static and pulsatile conditions.

The requirements of the testing apparatus are:

- A pulse duplicator that is able to produce physiological waveforms at different pressure levels;
- Simulations of relevant cardiac chambers and vessels dimension, which are considered relevant is however not specified;
- Chambers that allow visualization.

It is mentioned that compliance should be reproduced when relevant, but the only specific case presented is that of aortic compliance for unstented biological aortic valve.

The standard provides the pressure values that should be tested for hypotensive, normotensive, hypertensive and severely hypertensive conditions, the cardiac output values, systolic duration and acceptable results for different valve positions [4].

According to this Standard, test benches for aortic and mitral valves are composed by a pulse duplicator, a ventricle, connection tubes and some type of compliance/resistance elements that can vary in the different systems. More often than not the tubes used are rigid and straight, very far from natural vessels. Some systems, like the ViVitro pulse duplicator, allow to mount a compliant aortic root to test percutaneous valves.

2.2. Test benches developed

Since no specific indications are given a huge variety of test benches is has been developed by researchers in experimental set ups worldwide; the ones available of the market instead are few, with the ViVitro one being by far the most used. A company that wants to validate their products can choose between a variety of commercial products. Some experimental test benches have been fabricated by different institutions for research projects. The current lack of homogeneity calls for a specific study of the influence of the testing apparatus on the results in order to allow a useful comparison of devices [17].

2.2.1. Test benches on the market

The most used commercial test bench is the ViVitro Pulse Duplicator, composed by a pump, a model left heart, a flow measuring system and a data acquisition system. The heart model is composed by rigid structures, but two accessories are available to mount on the test bench to reach more physiological conditions: a viscoelastic impedance to better reproduce ventricular pressure and a compliant aortic conduit. The use of the latter is recommended for percutaneous prosthesis [17].



Figure 2.1.1: Pulse duplicator



Figure 2.1.2: Compliant aortic conduit

Figure 2.1: ViVitro standard set up with compliant accessory

Another commercial apparatus is the HDTi-6000 Heart Valve Pulse Duplicator by BDC Labs. This apparatus allows a great control on the pump waveform but is composed of rigid elements with the possibility to control the heart chamber compliance with air volumes [18].

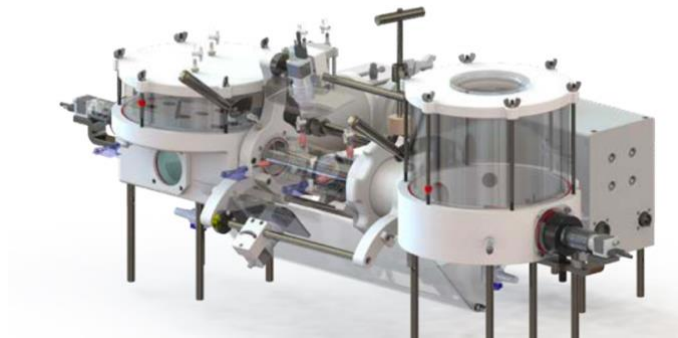


Figure 2.2: BDC Labs Pulse Duplicator

2.2.2. Test benches developed by different researchers

Researcher often produce their own pulse duplicators in order to obtain the precise structure needed for their tests.

Bazan and Ortiz developed a pulse duplicator characterized by adjustable compliance and resistance representing the systemic characteristics and with a model of the aortic tract with the enlargement of the Valsalva sinuses and an arterial impedance based on a Windkessel model [19].

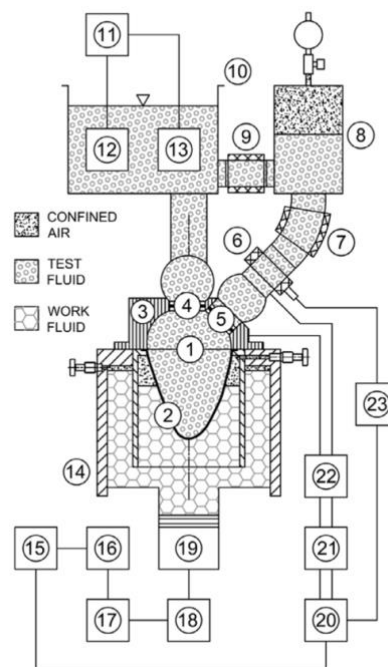


Figure 2.3: Cardiac simulator; 8 and 9 are the adjustable compliance and resistance while 7 is the aortic impedance

As another example at the Eindhoven University of technology they developed two different pulse duplicators. The first one is based on a system of compliance and resistances similar to the one described above but with the aorta modeled with an EPDM rubber. The second one, instead, has the test section placed on a base that moves vertically, simulating the heart movement in vivo [20].

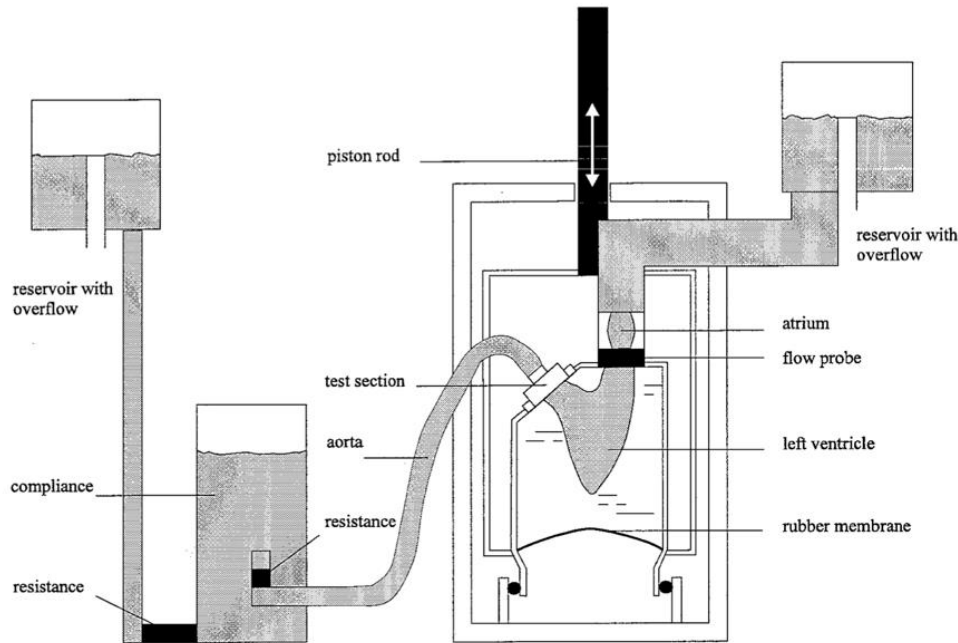


Figure 2.4: Test bench with vertically moving base to reproduce the fluid dynamics given by heart movement

The test bench used for this work has been previously developed at Politecnico di Milano for testing of a polymeric heart valve prosthesis. It is composed by:

- Volumetric pumping system representing the heart
- Ventricular chamber
- Aortic valve housing where the different prosthesis will be placed
- Resistance-Compliance-Resistance system that work as a systemic impedance simulator of the cardiovascular system
- Reservoir simulating the left atrium
- Mitral valve housing where a polymeric valve will be kept constant

The pumping system is connected to a software to produce different waveforms. The pump pushes a work fluid that, through a membrane, gives energy to the test fluid [10].

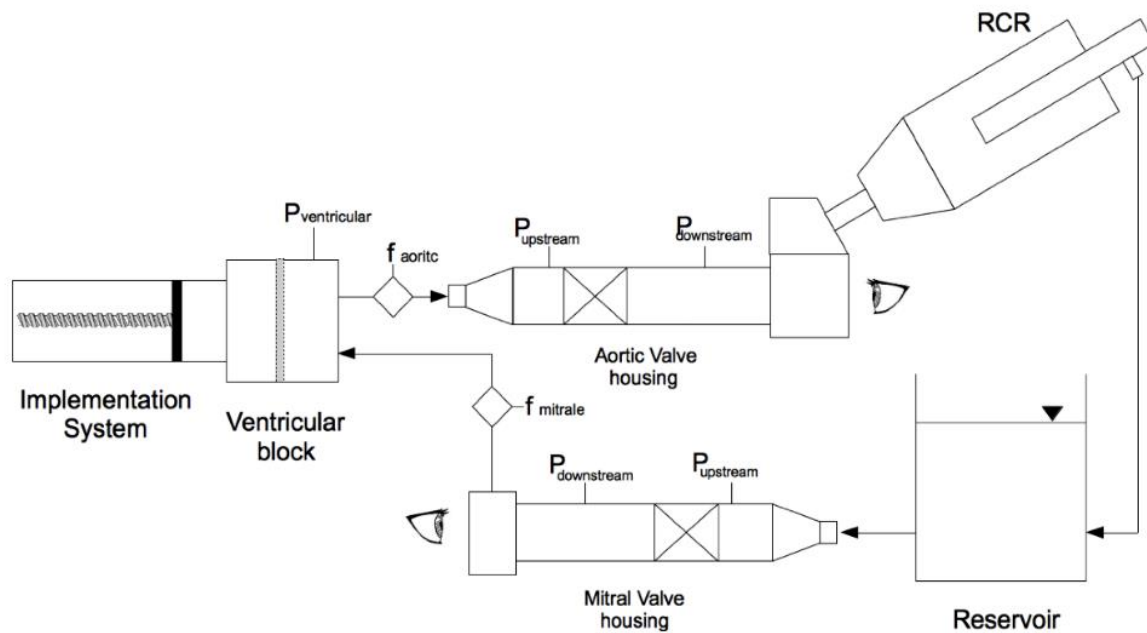


Figure 2.5: Schematic representation of the pulse duplicator used in this work

2.2.3. Aortic models

Besides them not being generally used to test aortic valves several models for the whole aorta and for some single tracts exist. They are generally produced by either casting or 3D printing, some models also exist where the casting mold is produced by 3D printing and then used to make several models [21]. With the continuous improvements of 3D printing that allow for better precision and finishing is becoming more and more convenient to use this technique to produce models since only few pieces are needed, not justifying the construction of a mold.

The most commonly used materials are silicon rubbers since they seem to well replicate the compliance of the aorta [5].



Figure 2.6: Compliant silicone aortic model

An example of aortic model used in a pulse duplicator can be found in the experimental setup developed in Eindhoven where an EPDM rubber was used to fabricate the aortic portion of tubing [20].

3 Polymer characterization

3.1. Properties of the natural aorta

The focus of this work is to replicate the mechanical behaviour of the natural aorta. In order to accomplish that, compliance was picked as our target property. A hollow body's compliance is defined as the increase in its internal volume over the increase in internal pressure:

$$C = \frac{\Delta V}{\Delta P}$$

In the years many studies have been performed to measure the aortic compliance, mainly with the objective to better understand the mechanism that leads to the formation of aneurisms. The techniques used in these studies are several but can be divided into two categories: mechanical testing performed on aortas harvested from cadavers and transoesophageal echocardiography performed during routine cardiac exams. While the first allows to perform a more complete mechanical analysis, the second has the advantage of evaluating the performance of the vessel *in vivo*. Given the different techniques used, and the fact that we are dealing with a biological tissue, that has intrinsically variable mechanical properties, the results found in literature can be very inhomogeneous. Moreover, the compliance changes significantly between the different regions of the aorta. In this work we focus mainly on the aortic root since is the most significant tract for the study of the aortic valve. After a complete analysis of the literature the value of 1 ml/mmHg has been found in an echocardiographic study [15] and with a direct study *in vivo* [16]; this value will be used henceforward for the conduit's design.

Since the compliance is dependent on the geometry, intrinsic properties needed to be considered for an initial material's selection. To achieve the final result, the elastic modulus of the artificial material will be measured and used to calculate the geometry to obtain the target compliance. Moreover, being the aorta an anisotropic material, we focused on reproducing its circumferential properties. The aorta is reported to have a tensile strength of 2 MPa and an elongation at break of 200% [22].

In conclusion the aim of this testing campaign was to gather information on the polymeric material of choice, in order to properly create and use the conduit for testing of different aortic valve's prosthesis.

3.2. Materials and methods

3.2.1. Choice of resin

For our work we wanted to exploit 3D printing. Before starting to prepare a specific resin in the lab we decided to explore the offer on the market. In particular we found that Formlabs (Formlabs Inc., Somerville, MA, USA) presented two soft resins: the Elastic 50A and the Flexible 80A; both could be used with the Form 3B+ printer already present in the laboratory. The 50A was selected as our top candidate since it had a reported tensile strength of 3,23 MPa and an elongation at break of 160% [23], close enough to the properties of the natural aorta. This resin, a copolymer based on acrylate monomers, is moreover indicated as having silicon-like properties that should be similar to those of most of the existing aortic phantoms.

3.2.2. Sample production

All samples used were produced with 3D printing, following the same procedure that will be used for the conduit fabrication. First a CAD model was created in SOLIDWORKS, then an STL file was exported in PREFORM, where orientation and support's placement were defined. The Form 3B+ printer was then used to obtain the samples. This printer works by stereolithography: the plate is dipped in the resin tank, polymerization of the resin with a laser is performed, according to the model, and then the plate is lifted in order to move on to the next layer. The deposition results in layers parallel to the printing platform.

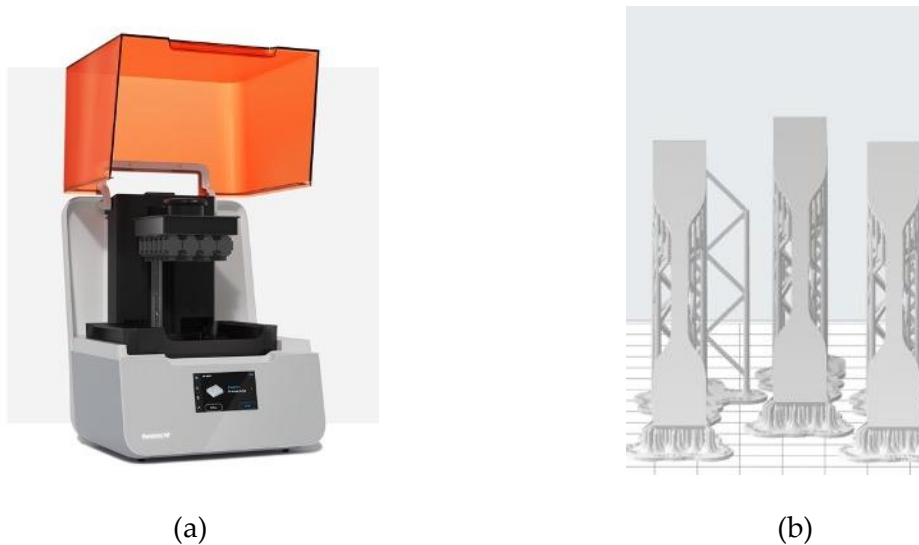


Figure 3.1: Printer (a) and printing example (b)

After printing the samples were rinsed for 20 minutes in isopropyl alcohol and cured in UV light at 60°C for 20 minutes, as indicated by the manufacturer in postprocessing instructions, to remove unreacted monomer and achieve optimal mechanical properties.

For all tests performed on the dynamometer the geometry of the samples was the dumbbell geometry described in BS ISO 37 [24]; in particular type 2 geometry was used since the thickness is close to the one of common aortic phantoms.

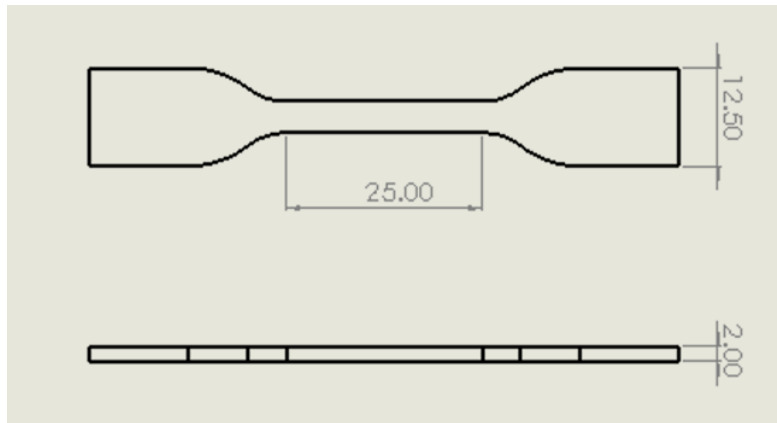


Figure 3.2: Geometry of uniaxial tensile samples

3.2.3. Tests

Swelling test

From the Formlabs datasheet the Elastic 50A resin has a reported swelling of 25.6% after 24h in 2-propanol; the fact that the resin swells and does not dissolve in the organic solvent indicates its crosslinked nature. Since our material will be in prolonged contact with water, and the knowledge of its behavior was of cardinal importance, a swelling test with water, 2-propanol, and toluene was performed. For this test 9 parallelepipedal samples with dimensions 5x5x10 mm³ were produced. Each of the sample was measured and weighted and then placed in a baker with 100 mL of solution: 3 contained distilled water, 3 propanol and 3 toluene. The bakers were placed under an air-flow hood and covered to avoid solvent evaporation. Since we wanted to monitor the uptake for prolonged times the following time points were chosen:

Table 3.1: Time points of swelling test

Time point	1	2	3	4	5
Hours from 0	24	48	120	144	288

At each time point the samples were taken out one by one, weighted, measured, and then placed back in the solutions.

Tensile test

In order to properly design the conduit, the elastic modulus over a range of stresses was needed. To rapidly obtain that, ramp tests were conducted on the dynamometer. These tests were also used to verify the stress and strain at break reported in the producer's datasheet and confirm the material choice. The obtained value of the Young modulus was used to calculate the thickness that the tube ought to have in order to reach the desired compliance.

Tensile tests were performed on 6 specimens using a INSTRON 5967 machine, equipped with 2 pneumatic gouges and a 2kN load cell; the INSTRON software was used to collect force-displacement curves. The tests were performed with a displacement rate of 500 mm/min up to rupture. Since, due to the dumbbell shape and the compliant nature of the material, the strain state would be inhomogeneous, instead of using the recorded displacement the strain was evaluated with an optical system. The optical system was composed by a Nikon 28-105 camera with a 10 MPixel ueye optic. During the experiment the camera was used to collect a video of the sample; in particular the test length, marked on the sample, was to be always in the frame. The videos were then analyzed frame by frame with ImageJ software in order to obtain the distance between the two marks of the test length. From the analysis of the distance the strain in each frame was obtained considering the first frame as initial length. Then OriginLab software was used to construct stress-strain curves for each sample. Moreover, the same software was used to find a mean stress curve between the samples. This data was then used to approximate the Young Modulus by taking the derivative of the mean stress as a function of strain from 0 up to rupture. This derivative was then fitted with a polynomial function and this function was implemented in a Matlab code. In a different code, first the compliance and pressure difference were combined to find the desired change in volume; considering a constant length the area variation is:

$$\Delta A = \frac{C}{l} * \Delta P$$

At this point the area variation was correlated to the known quantities starting from the definition:

$$\Delta A = \pi * (r_2^2 - r_1^2)$$

Then the radii were correlated to initial radius and strain by:

$$r = r_0 * (1 + \varepsilon)$$

The stress and strain were correlated by the elastic relationship through the Young Modulus's function, previously obtained:

$$\varepsilon = \frac{\sigma}{E}$$

Then from the physiological pressure values, oscillating from 80 to 120 mmHg, the circumferential stresses in the tube were obtained using Mariotte's law:

$$\sigma_{\vartheta} = P \frac{r}{t}$$

where P is the internal pressure, r the radius and t the thickness.

The resulting equation for the area variation is:

$$\Delta A = \pi * r_0^2 * \left[\left(1 + \frac{P_2 * r_0}{E_2 * t} \right)^2 - \left(1 + \frac{P_1 * r_0}{E_1 * t} \right)^2 \right]$$

Since our goal was to calculate the thickness, an iterative process starting from an initial guess of 1,5 mm was used.

In order to see the change in stress-strain behavior due to different displacement rate, two additional samples were tested at 100 mm/min and compared with the other ones.

Isotropy

Since the process of 3D printing could introduce an anisotropy in the final product, a series of tests was conducted to see if the result would be isotropic. This was of particular importance since the dimension of the build platform are limited and the orientation of the conduit during printing will be heavily constrained.

For this test 3 orientations were considered: vertical (V), horizontal (O), and parallel to plate (S). For each 3 dumbbell samples were produced and the results were also compared with the results of 3 diagonal (D) samples previously tested for the tensile test. The tests were executed exactly as described above at the elongation rate of 500 mm/min.

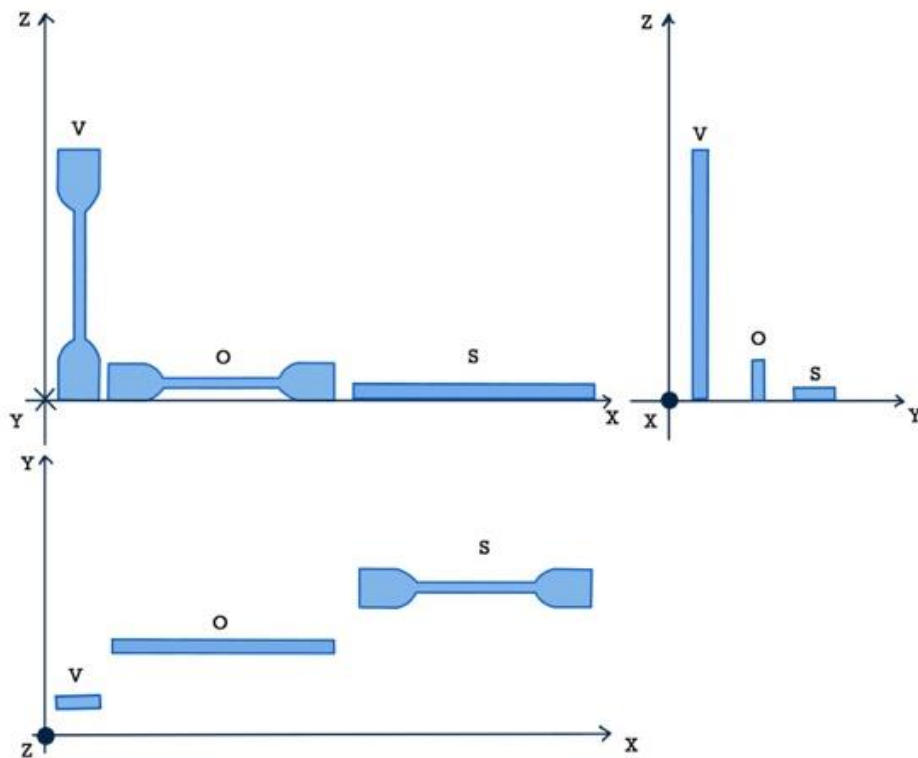


Figure 3.3: Schematic representation of the different orientations. The printing plate is the x-y plane, the plate moves along z while the laser radiates along y and then advances along x

Creep test

Since the material is polymeric and likely viscoelastic it was important to analyse the viscoelastic transition. In order to do that a creep experiment was set up. The dynamometer was used to hold and load the sample: on the upper side a 500 N gauge was placed to hold the sample while on the lower side of the sample a weight of 359.7g was placed. The lower bar of the dynamometer was used to hold the weight, so that the load started being applied to the sample when it detached from the bar. In order to gather frequent data at short times and less frequent at longer times a double optical set up was used: a video was acquired for the first 3 minutes with the Nikon 28105 and 10 MPixel ueye at 50 Hz while a camera was used to take a picture every 30 s until the end of the experiment. The images were then analysed in the same way as the ones from tensile tests and elaborated as to eliminate the differences in light absorbed and zoom. From the strain values the creep compliance was calculated considering the weight applied and the sample's initial area.

Assessment of the linear behavior range

In order to have a deeper understanding of the material’s behaviour, a campaign of tests was dedicated to find the linear viscoelasticity region and to observe the entity of the viscoelastic transition. If, for example, our working conditions were to be outside the linear region the compliance would change with the stress level, and it would be important to optimize it for the service conditions.

It was decided to perform 6 stress relaxation experiments on the DMA apparatus in the following conditions; with the acquisition frequency for stress of 1 Hz.

Table 3.2: Testing conditions for linearity experiment

Test	1	2	3	4	5	6
Imposed strain (%)	0.1	0.5	1	2	5	7

The recorded stresses were then used to construct 6 isochronous curves to show whether the material was linear or not.

Pressurization test

After calculating the theoretical pipe thickness, a sample conduit having this specific thickness was produced and subjected to a pressurization test.

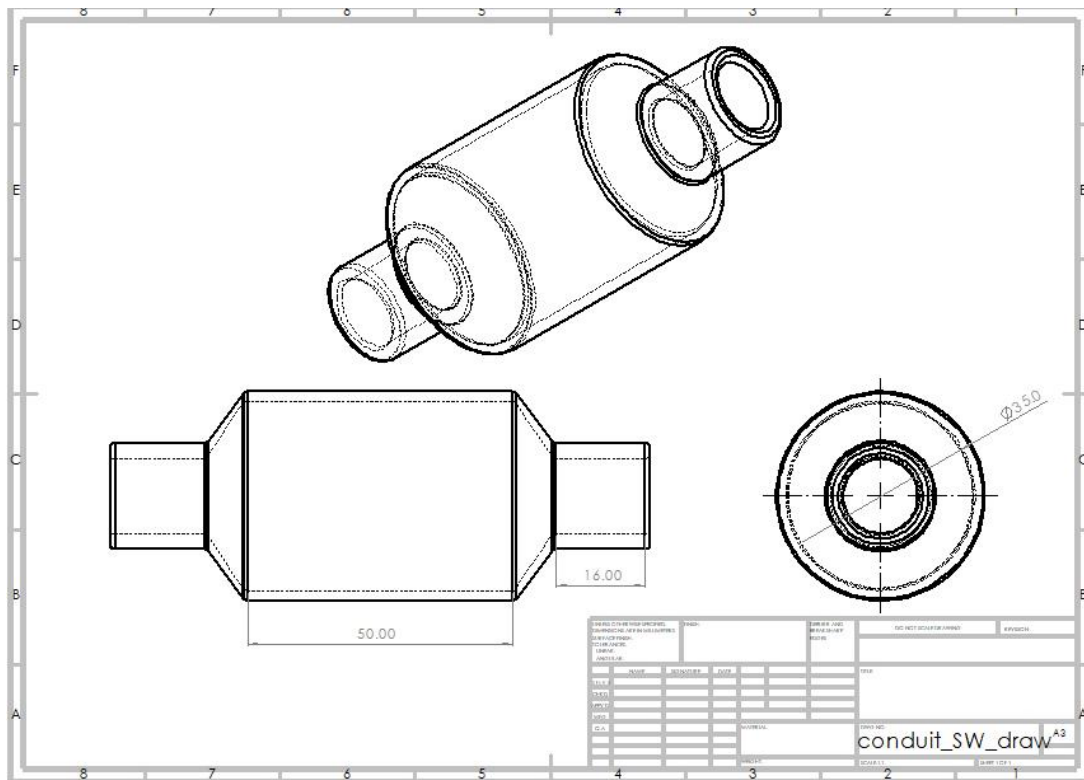


Figure 3.4: Section of the conduit

To perform the test both ends were connected to a rigid piping system with one access per side.



Figure 3.5: Experimental set up

On one side a pressure sensor was connected while the other was used to add water with a syringe. Starting with the filled conduit at 0 mmHg water was added at 2 mL intervals while the pressure was recorded. The process was repeated 3 times. The pressure values were averaged and from the added volume the area variation was calculated. Then the length normalized compliance was estimated as the area variation over pressure variation; this was done in order to obtain information independent from the length of the pipe. Before testing it was checked that the edge tubing and connectors were rigid and therefore their compliance could be neglected.

Cyclic tests on dynamometer

As a first analysis of the dynamic properties of the material, cyclic tests were performed on the dynamometer at a frequency reduced from the 70 bpm expected in service due to limitation of the instrument. The tests were performed with the same set up used for the tensile tests. For the first test a strain between 0 and 100% was applied up to rupture at 100 mm/min. On the second sample, instead, 350 cycles between 0 and 25% strain were performed at the same strain rate. The number of cycles was determined by considering a 5-minute test at the physiological frequency of 70 bpm; this number will also allow us to comply with the Standard [24], that requires to collect data for at least 15 useful cycles.

Cyclic tests on DMA

In order to gather information on the behaviour at the real exercise frequency the testing was moved to the DMA apparatus to overcome the velocity limitation of the dynamometer. Each test lasted 25 minutes and the testing conditions are as follow:

Table 3.3: Testing condition of cyclic DMA tests

Sample	Static (%)	Dynamic (%)	Frequency (Hz)
1	5.75	1.25	1
2	5.75	1.25	1
3	5.75	1.25	1
4	5.75	1.25	2
5	5.75	1.25	2
6	5.75	1.25	2
7	5.75	1.25	5
8	5.75	1.25	5
9	5.75	1.25	5
10	10	3	1
11	10	3	1
12	10	3	1
13	10	3	2
14	10	3	2
15	10	3	2
16	10	3	5
17	10	3	5
18	10	3	5

The testing conditions were determined considering the normotensive, 80 to 120 mmHg, and hypertensive, 120 to 210 mmHg, testing conditions.

In addition, to explore a wider frequency range and check for influence of previous testing, samples 9 and 18 were subjected to frequency sweep test before and after the cyclic test.

Time dependence

Since during the testing of the cardiac valves the conduit will have to be used for several days, it was decided to test whether or not the properties would be affected by time. In order to do that, the whole batch of samples was produced at the same time, then they were divided into groups of 5, and each group was kept in contact with air or submerged in water up to its own testing time. The decision to observe the aging process in air and water was taken due to the prolonged contact that the inside wall will have with water while the outside will be dry. All samples were tested in the DMA apparatus at 2 Hz; for each group 3 samples were tested at $5.75\% \pm 1.25\%$ and the last 2 at $10\% \pm 3\%$.

3.3. Results

Swelling

At the end of the experiment none of the samples showed signs of dissolution. It can be then concluded that the material is crosslinked. In toluene an increase in weight of 120% happened in the first 24 h and then remained almost constant, while in propanol the increase was more gradual and reached 100% at the end of the experiment. In water the material reached a 4.5% weight increase; indicating that a level of water absorption does happen. The volume of the samples has been calculated from the dimensions; due to the irregular surface of the samples, obtained after the removal of supports, these measures have low precision. They can, however, be used to conclude that not only solvent intake, but also swelling does happen. If a crosslinked polymer is put in contact with a compatible solvent, its molecules will migrate inside the material and stretch its chains, provoking dilatation. The process reaches equilibrium when the decrease in entropy, caused by the stretch, balances the increase in enthalpy, caused by mixing [25]. Water intake cannot be easily eliminated without altering material properties but will be considered when dealing with following material properties.

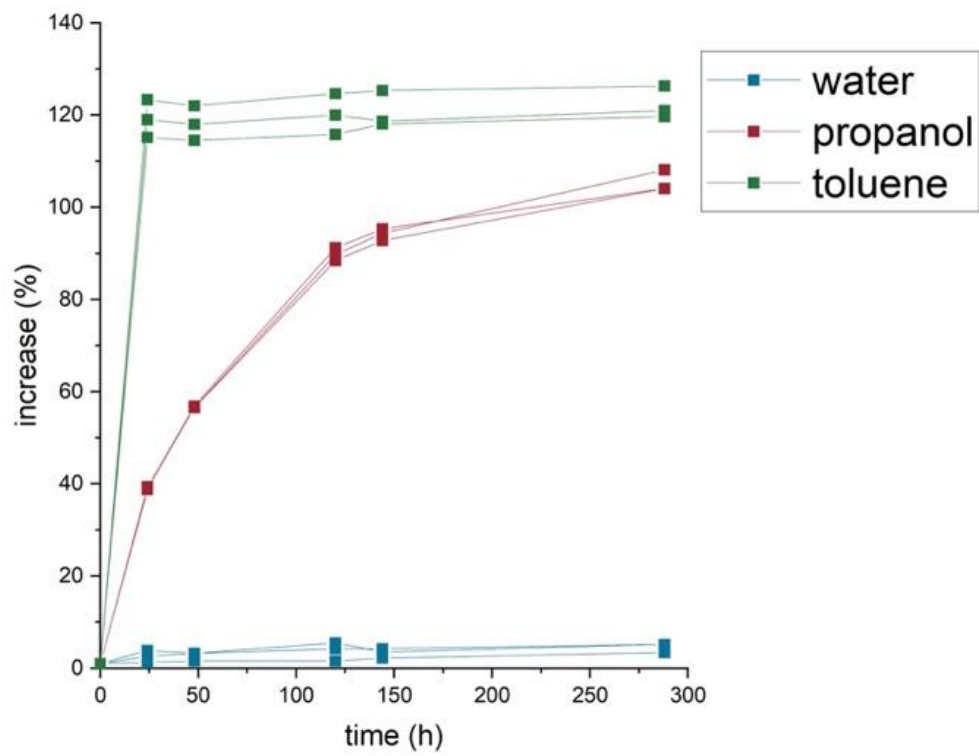


Figure 3.6.1: Mass increase

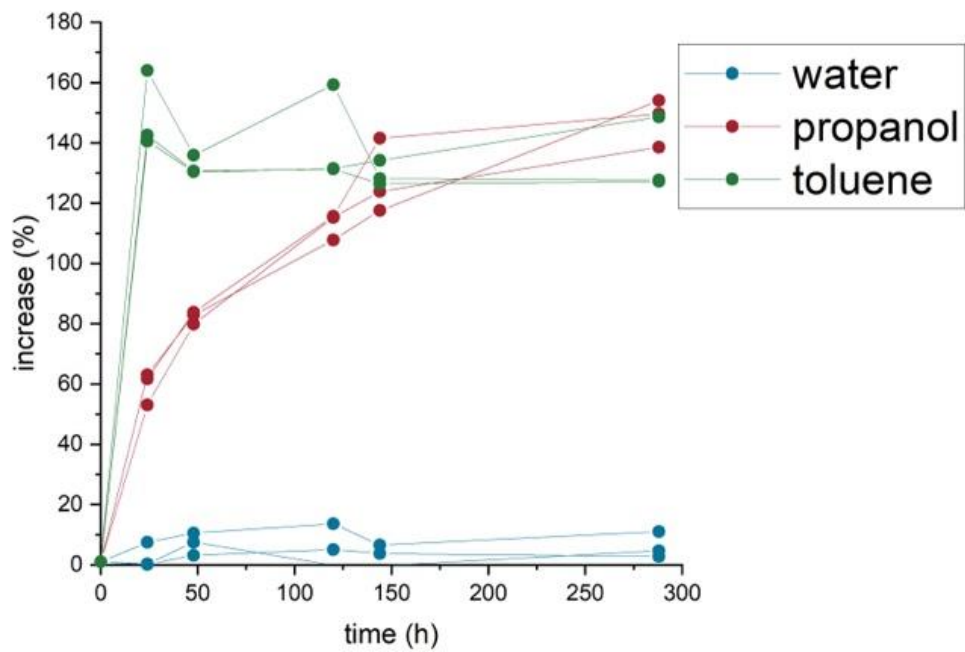


Figure 3.6.2: Volume increase

Figure 3.6: Percentage increase for samples during testing

Tensile

The mechanical behavior shown by the material is characterized by good repeatability with no significant difference between the two testing velocities. The first observation that can be done is that the values of theoretical stress and strain at rupture, 3.23 MPa and 1.6 respectively, are almost reached by the material, confirming the initial material choice. The slight underperformance shown by the material can be explained by the fact that additive manufacturing introduces a microgeometry, related to specific printer and resin characteristics that do not have perfect repeatability [26]. In this case it has been noticed that some microbubbles appear in the resin tank that, if embedded in the material, may justify the strength reduction. A region of direct proportionality between stress and strain can be identified under 0.25 strain; after that the deformation is non-linear up to rupture. The nonlinear region can be divided into two: in the first one the slope decreases while in the second one it increases. The first region can be explained by the alignment of macromolecular chains, limited by the presence of cross-links. The second region, instead, corresponds to stretch of single chains. When also this process reaches its limit, the material fails; this type of behavior is typical of elastomers.

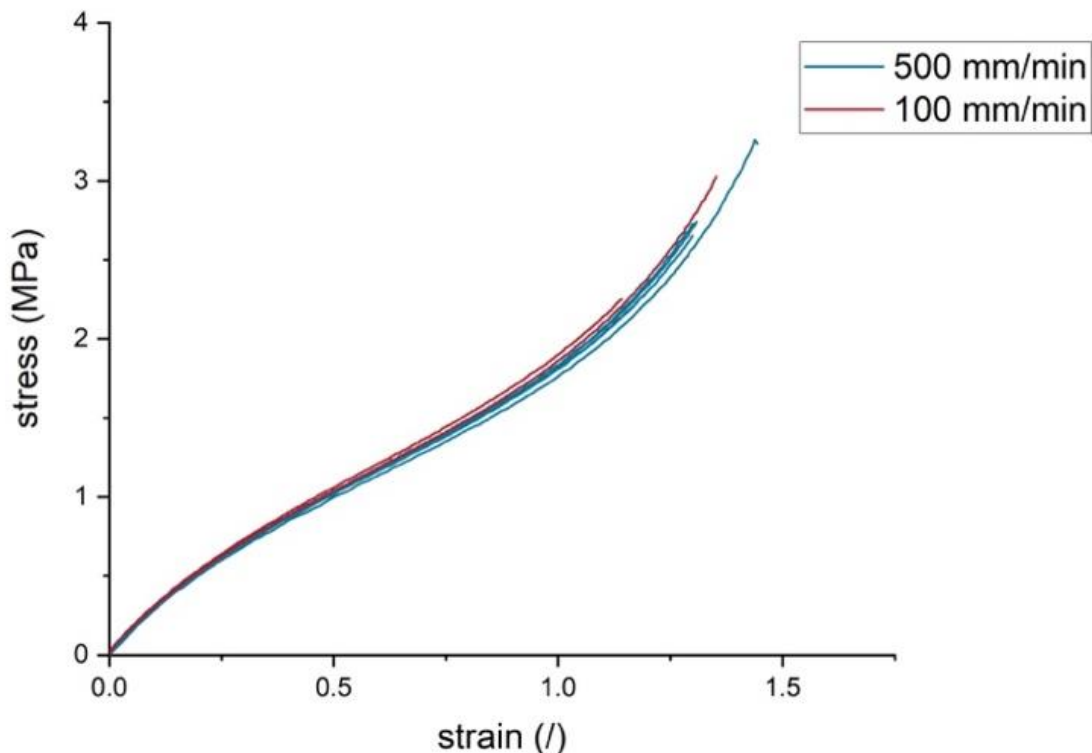


Figure 3.7.1: Curve for each sample tested at the two different velocities

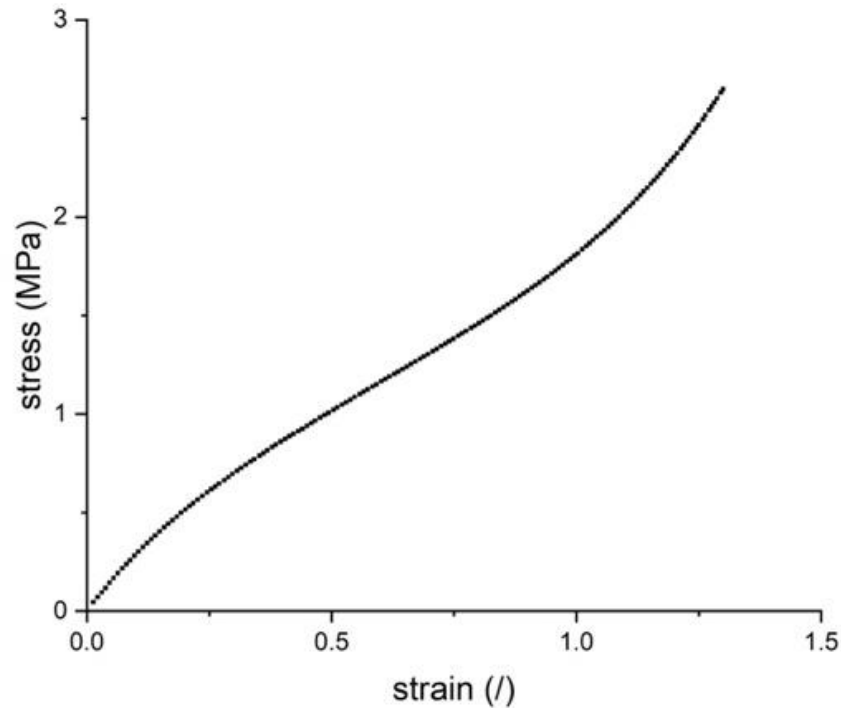


Figure 3.7.2: Average curve

Figure 3.7: Stress-strain curves obtained from tensile test

After the data processing and mathematical calculations, the required thickness to reach target compliance when oscillating from 80 to 120 mmHg, normotensive condition, in internal pressure is 1.82 mm. The resulting stress variation will be from 0.103 to 0.154 MPa while the strain variation will be from 3.5% to 5.5%. If the hypertensive conditions, of 120 to 210 mmHg, are considered with the same thickness, the stress variation will be between 0.154 and 0.269 MPa while the strain one is 5.5% to 10.5%

Isotropy

The samples printed along different directions follow curves with the same slope. There is, however, a difference in the maximum strain reached. In particular 2 of the S samples and one O fail at roughly 0.65 strain. While a V sample shows longer failure elongation than the others. Sample V1 was excluded from the analysis since it broke outside the testing length.

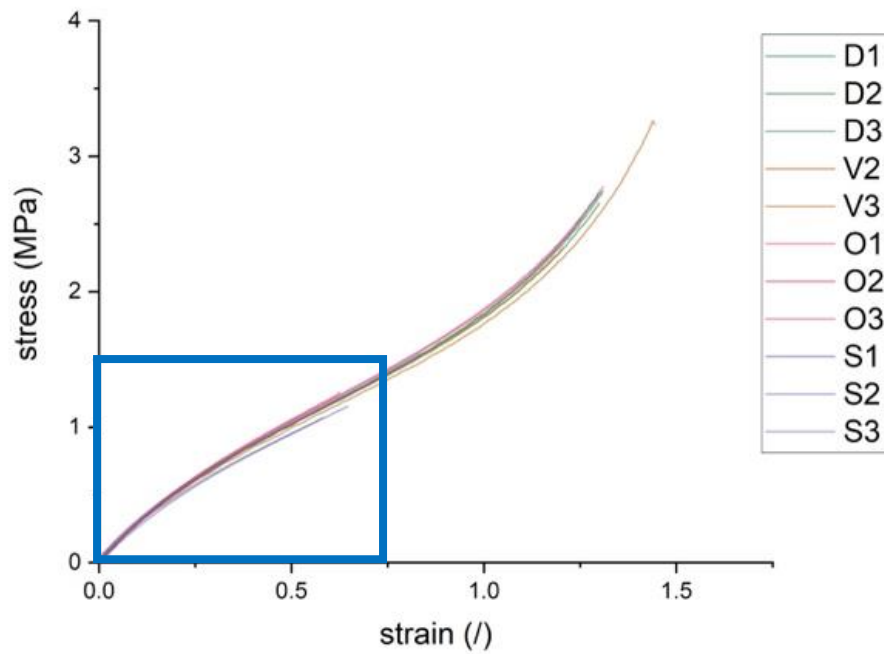


Figure 3.8.1: Curves for all the samples; V1 excluded

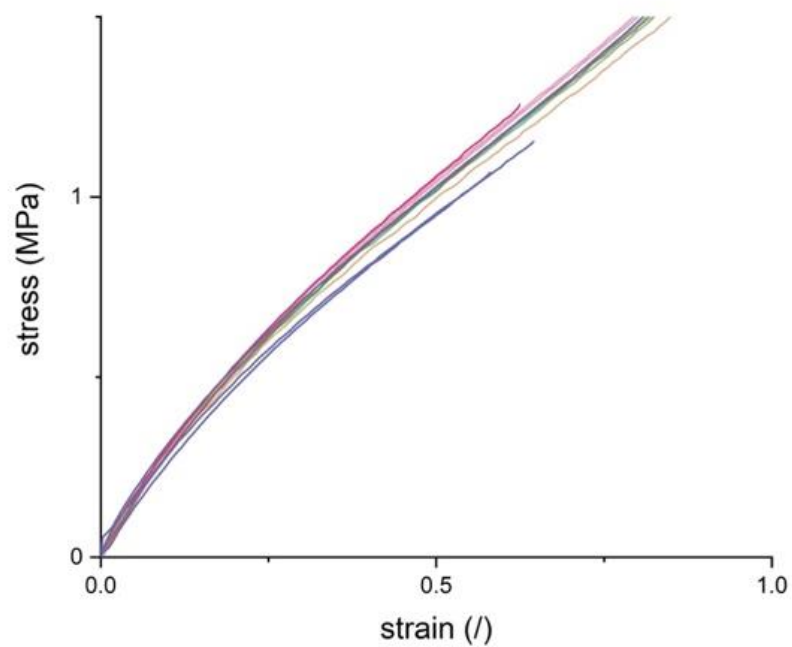


Figure 3.8.2: Focus on O and V sample with reduced strength

Figure 3.8: Stress-strain curves for samples printed in different directions

The differences in strength are not related to the sample itself but to post processing. In 3D printing the samples require supports in order to be printed properly, the placement of this supports is crucial and the lack of them leads to failure of prints. For the Elastic 50A resin the removal of this support is quite complex since they need to be pulled slightly to obtain a stretch and then cut as close as possible to the sample. The removal is done by hand and becomes particularly hard in regions were multiple supports are placed closely and can easily lead to the introduction of defects.

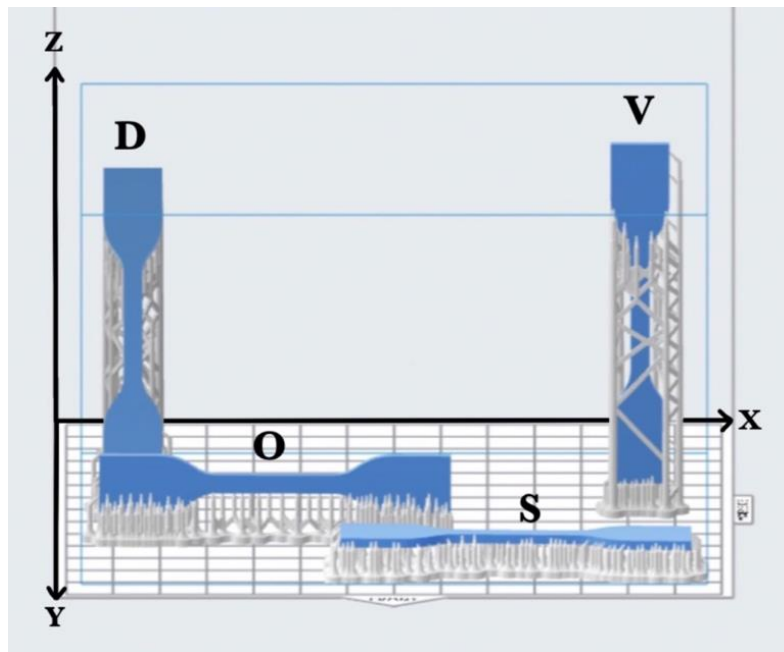


Figure 3.9: Printing chamber positioning for isotropy tests

As visible in the picture the S geometry required a high density of supports with attachment points on the test length, while the V geometry had very few supports and well-spaced. It can be then concluded that the printing process itself is isotropic and that placement of supports, with their removal, plays a crucial role in the final properties.

Creep behavior

In figure 3.12.1 the loading curve of the experiment is shown. The force reaches its maximum in around 8 seconds. In order to measure a creep response replicating the one reached by an ideal step loading the observation time for the compliance starts at 80 s. As visible in the graph the compliance is constant in this time. This does not mean that no viscoelastic transition happens for this material but simply that it is over before the observation time starts. It was not possible to apply a faster ramp so this is the only result obtainable from this test.

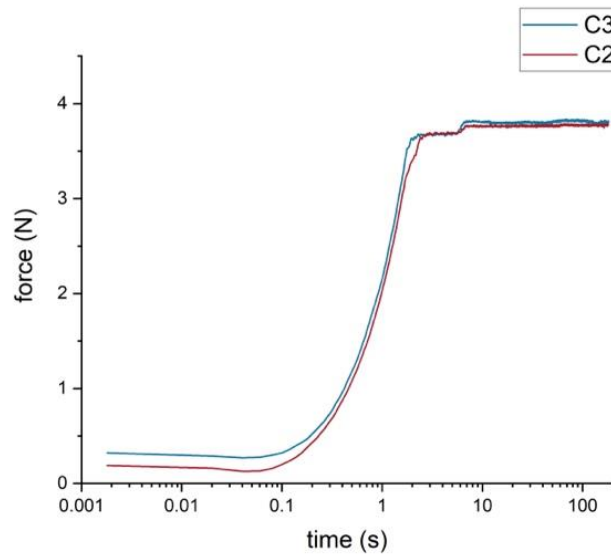


Figure 3.12.1: Loading curve

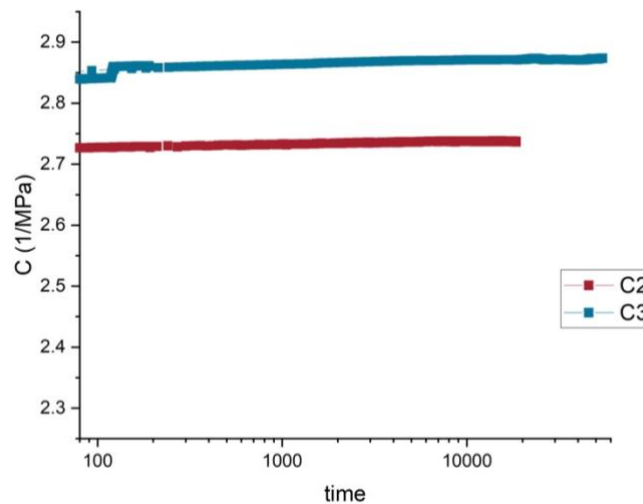


Figure 3.12.2: Registered compliance as a function of time

Figure 3.10: Results of the creep experiment

Assessment of the linear behavior range

The first thing that can be observed in the stress relaxation curves is how the Young modulus decreases going from 1% to 7% applied strain. The non-linearity is confirmed by looking at the isochronous curves, where the linear viscoelastic approximation can clearly no longer be applied after 1% strain. Another interesting fact to observe is the overlap of the isochronous curves for times above 100 s; this implies a fast viscoelastic transition, in which the modulus, at the different strains, is constant after roughly 100s, coherently with the result of the creep test.

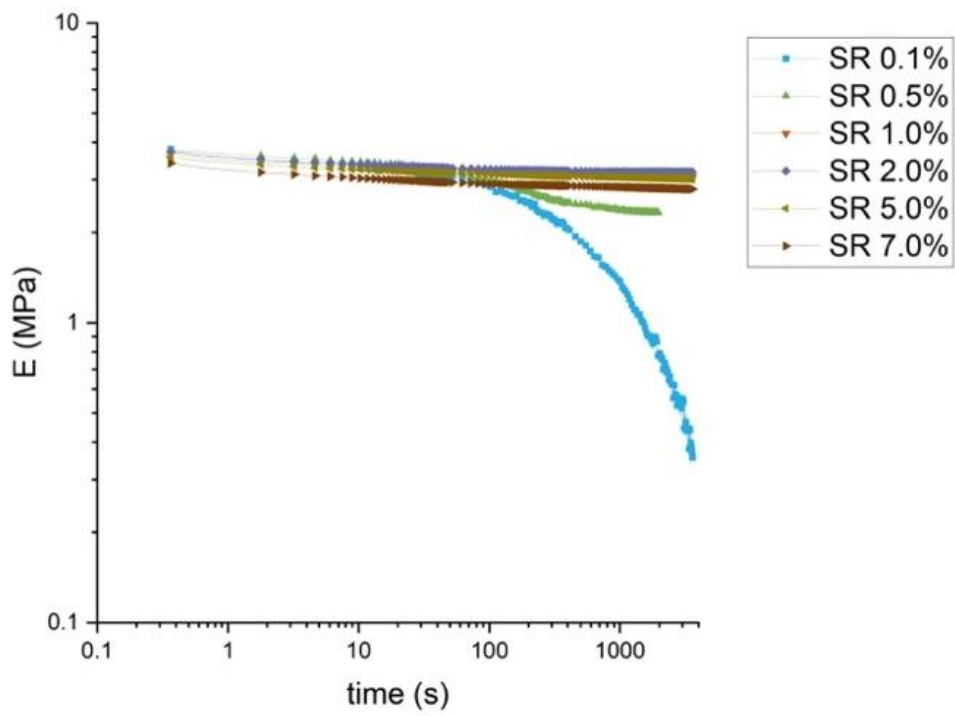


Figure 3.10.1: Young modulus curves

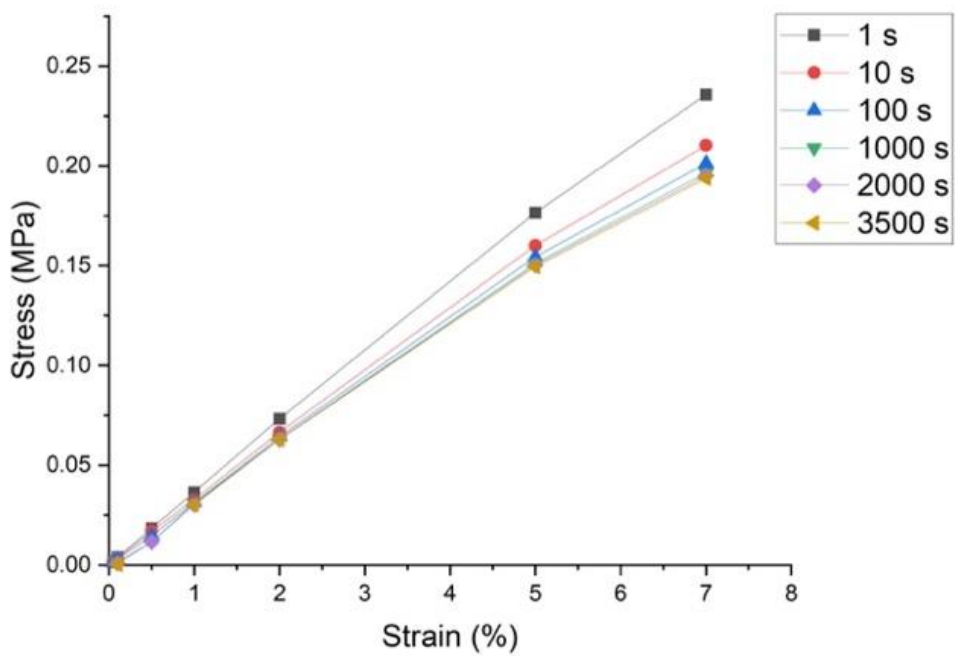


Figure 3.10.2: Isochronous curves

Figure 3.11: Results of stress relaxation experiment

Effect of the applied internal pressure on the pipe

The normalized compliance is not constant in the pressure interval tested; since from the linearity tests we saw the elastic modulus decreasing for increasing applied strain above 1%, it is natural to see the increase in compliance when the radial strains are above that limit. If the compliance is analyzed against internal pressure, it can be seen how in the interval of normotensive pressures the target compliance of 0.01 cm²/mmHg is reached within a 20% error. Since the compliance increases with pressure in the hypertensive condition the compliance will be the much closer to target value.

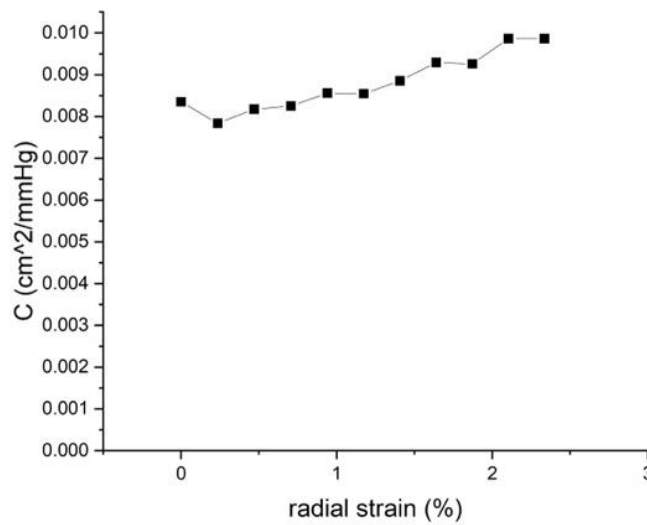


Figure 3.11.1: Normalized compliance as a function of radial strain

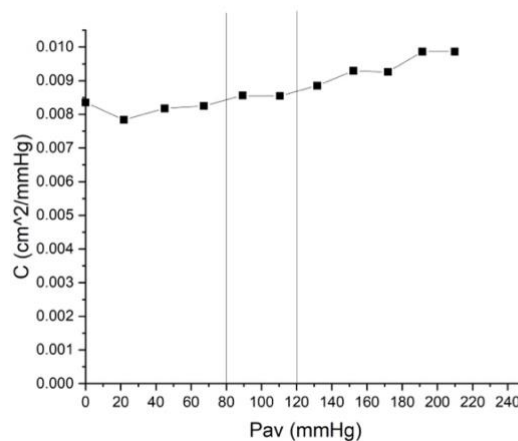


Figure 3.11.2: Normalized compliance as a function of internal pressure; the physiological range is marked

Figure 3.12: Results of the pressurization tests

Effect of cyclic loading

In the first test performed at 100% strain the sample broke at third cycle. The material shows a small hysteresis loop, implying a low dissipated energy and a residual deformation lower than 0.5% after each cycle related to almost null plastic deformation. This is to be expected in a crosslinked material since the links significantly reduce the amount of plastic deformation that can be reached. The low dissipated energy is instead an indication of a small viscous contribution; from this we can conclude that, besides being fast, the viscoelastic transition is small in entity.

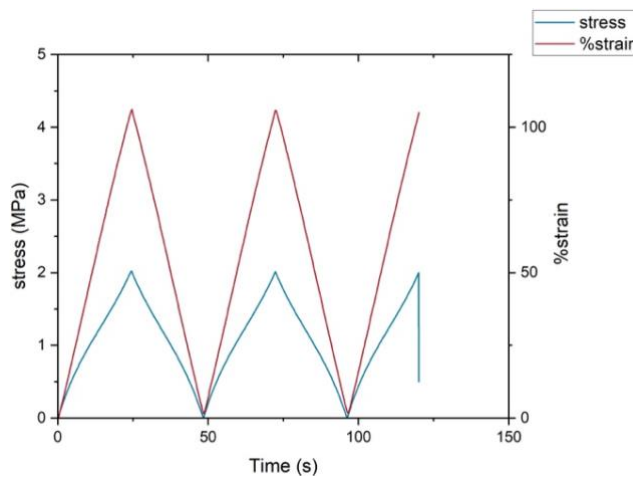


Figure 3.13.1: Stress and strain time behavior

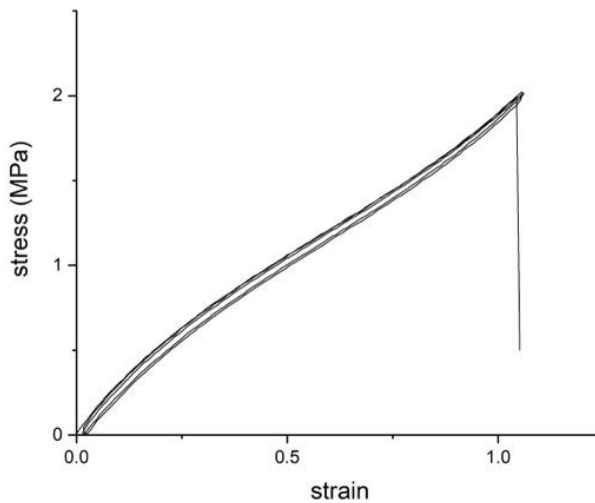


Figure 3.13.2: Hysteresis curve

Figure 3.13: Results of the cyclic experiment at 100%

During the second experiment, at 25% strain, the material was able to withstand 350 cycles; this numbers corresponds to 5 minutes of testing in the pulsatile apparatus at 70 bpm and complies with the standard of at least 15 cycles for characterization.

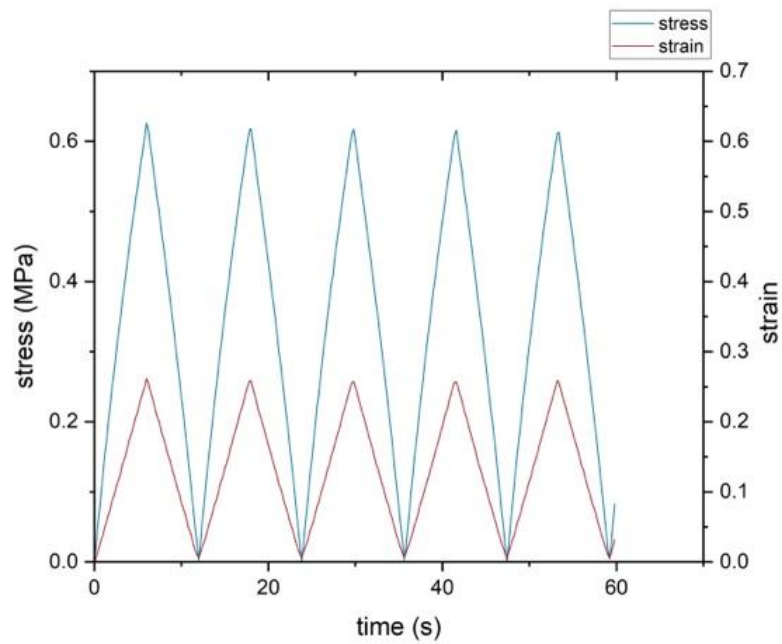


Figure 3.14.1: First 5 cycles

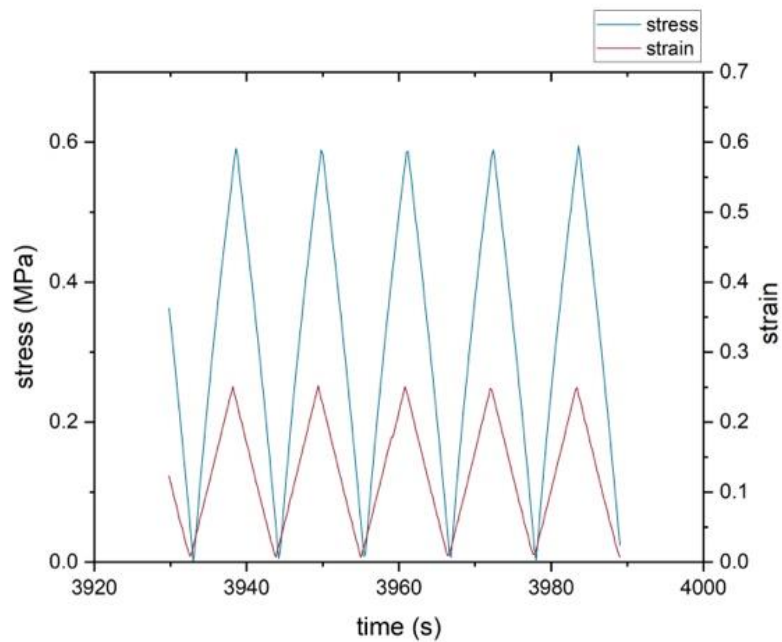


Figure 3.14.2: Last 5 cycles

Figure 3.14: Stress and strain time behavior at 25% strain

The residual strain after each cycle is small, with an average of 0.008, and constant: this is to be expected since the transition of the material is very quick implying a fast recovery and there is no accumulation of plastic strain. The maximum stress reached reduces of 5% due to a strain induced softening of the material during cyclic load.

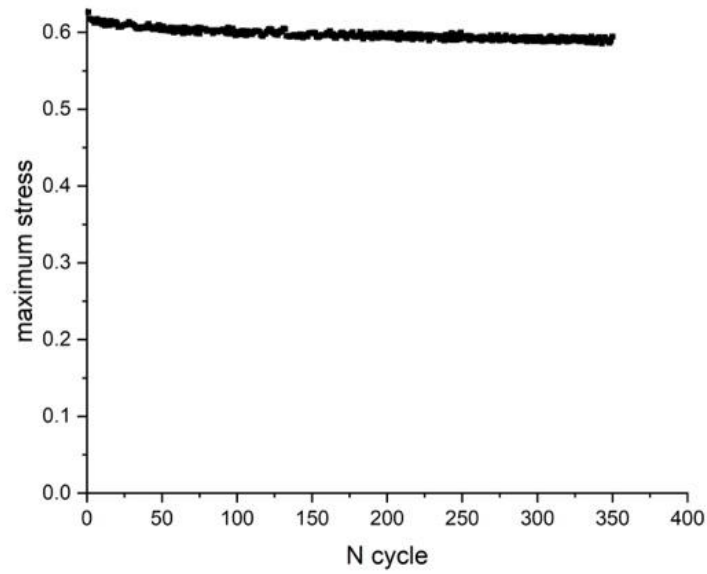


Figure 3.15.1: Maximum stress

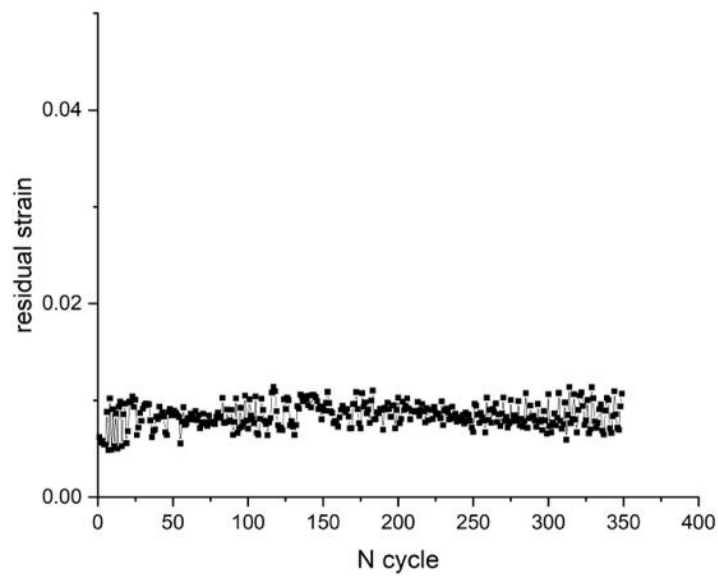


Figure 3.15.2: Residual strain

Figure 3.15: Cyclic behavior

Looking at the hysteresis loops we can see that during the first three cycles the dissipated energy is negligible, while it becomes significant at the end of testing. Since we saw a strain softening effect reducing the maximum stress, one possible

explanation for the increase of energy dissipation is some damage occurring in this stage.

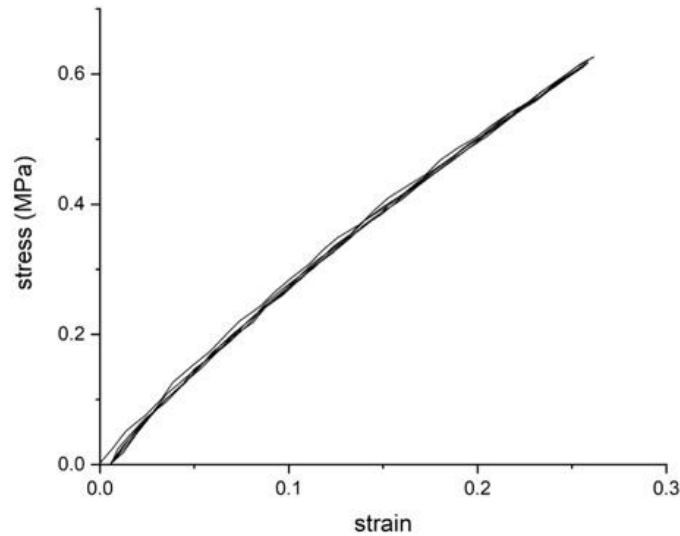


Figure 3.16.1: First 3 cycles

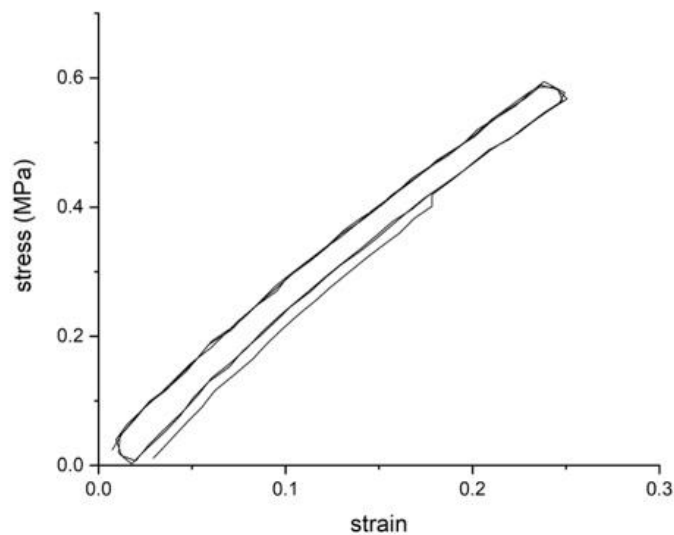


Figure 3.16.2: Last 3 cycles

Figure 3.16: Hysteresis loops at the beginning and end of the 25% strain experiment

There was no change with time during the DMA tests and the samples showed good repeatability in the same conditions. Because of this for each sample the average over time was calculated for both E^* and $\text{tg}\delta$; these values were then combined to obtain an average single value for each tested condition.

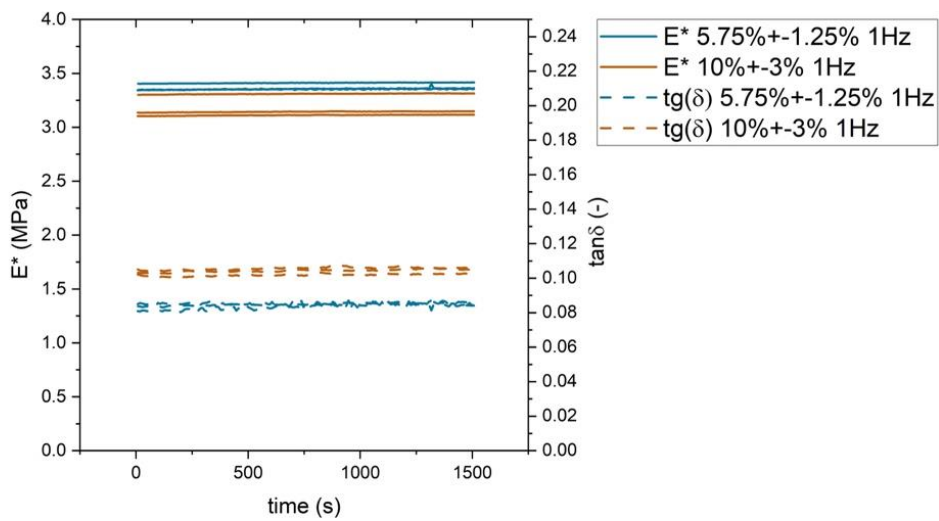


Figure 3.17: E^* and $tg\delta$ as function of time for 2 samples

Looking at the average values obtained as described above, we can see how with increasing frequency both the modulus and the $tg\delta$ increase, the second one more significantly. Since $\tan(\delta)$ increases with the loss modulus and decreases with the conservative modulus, while E^* increases with both, we can conclude that the loss modulus increases more significantly with frequency than the elastic one. Not much difference instead is shown in the two different loading conditions, especially at higher frequencies.

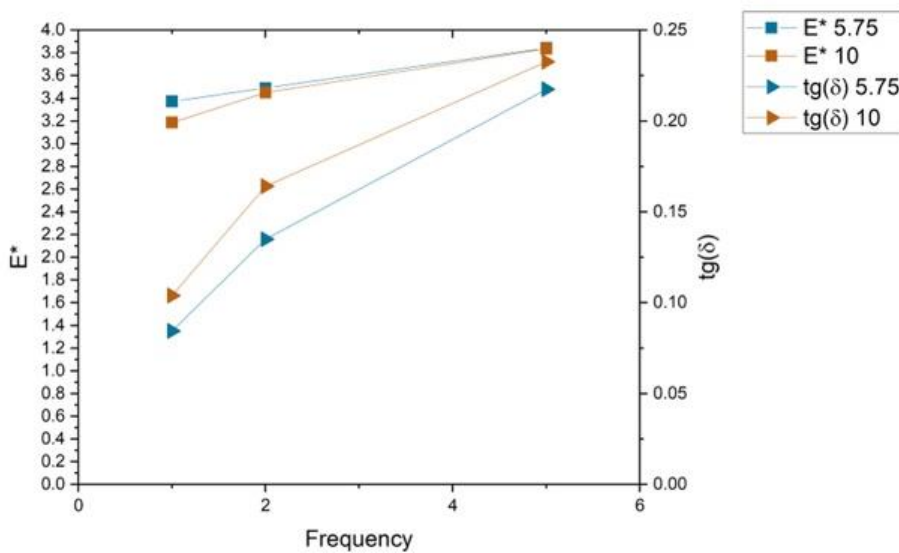


Figure 3.18: E^* and $tg\delta$ as function of frequency

By looking at the frequency sweeps we can confirm that both moduli increase with frequency, with the loss modulus increasing more significantly. We can also conclude that there is no difference between the samples tested before and after the cyclic test.

This is to be expected for a crosslinked elastomer with the low plastic deformation and short viscoelastic transition observed up to now.

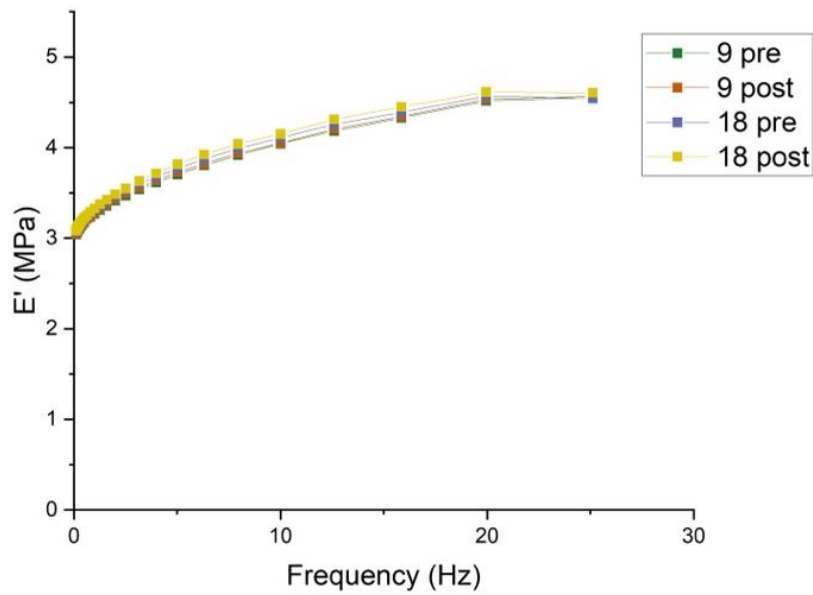


Figure 3.19.1: Conservative modulus

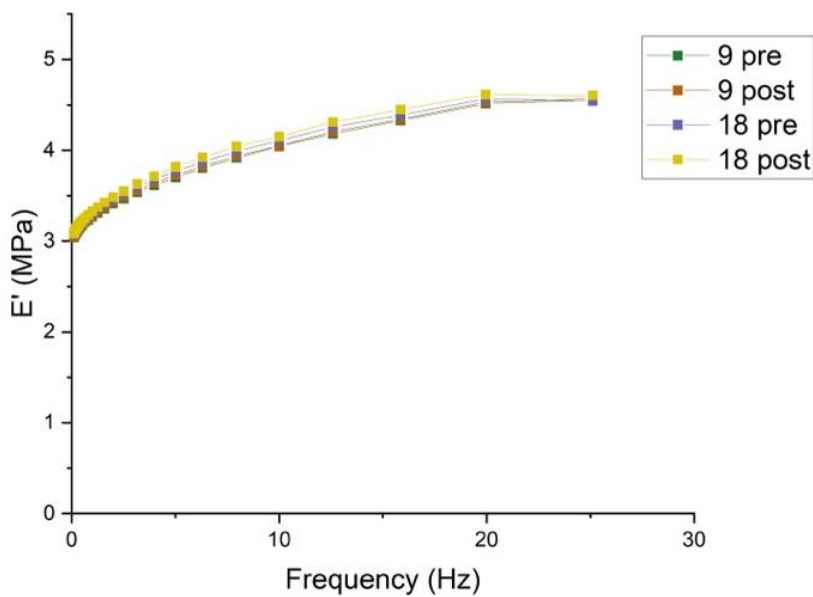


Figure 3.19.2: Dissipative modulus

Figure 3.19: Moduli in frequency sweep

Aging

The modulus increased in the sample in contact with air, while it is basically constant in the one in water. $T_g(\delta)$ increased in both cases but less in the samples immersed in

water. These results can be explained by an aging typical of UV crosslinked polymers: the unreacted monomer acts as a plasticizer in the material, with time the crosslinking reaction goes on and the effect of the unreacted material trapped inside decreases. The effect is less pronounced in water since water acts as plasticizer for the polymer and therefore partly compensates the loss of monomer.

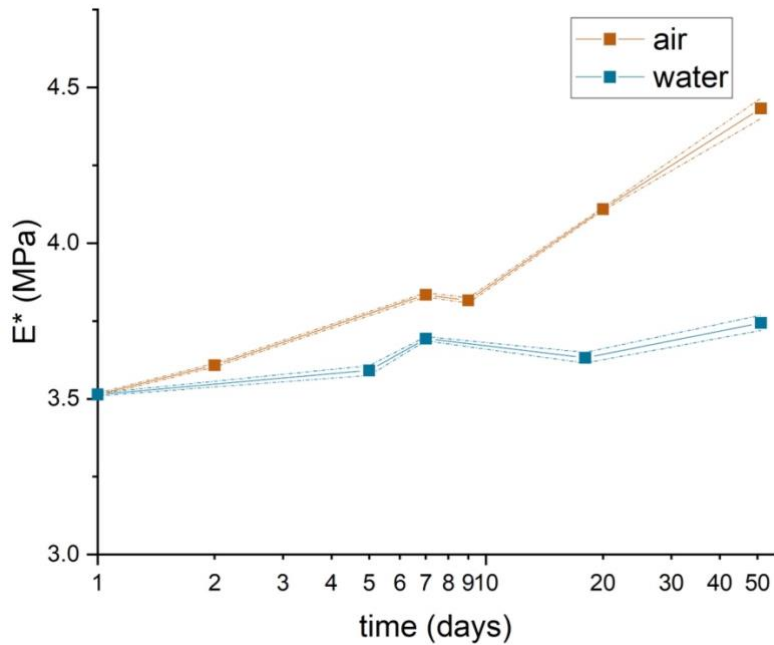


Figure 3.20.1: E*

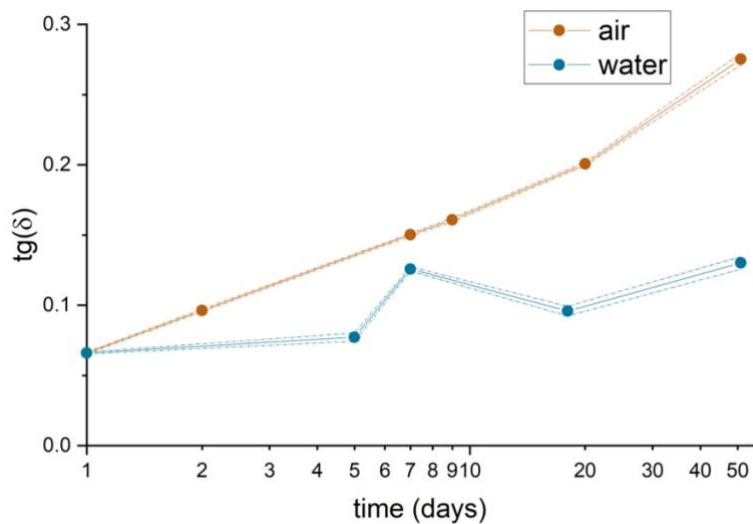


Figure 3.20.2: tgδ

Figure 3.20: E* and tgδ as a function of time, comparison between air and water

3.4. Final conduit design

The initially chosen resin was confirmed to be appropriate for the application. In particular a thickness of 1.82 mm was found through iterations starting from 1.5 mm and will need to be used in order to reach the compliance of 0.01 cm²/mmHg required. Since the material is isotropic the printing direction will be chosen based on best predicted process and supports placement. The cyclic tests predict that the material should not fail during service. Due to the results of the time dependence experiment it has been decided to perform all tests within 5 days of printing the conduit in order to avoid changes in the properties. In the event that a new testing campaign with the same compliant conduit were to be planned, it would be required to print a new conduit since the properties are expected to change significantly within a month.

4 Valve Testing

4.1. Aim

The objective of the following tests is to compare the performances of valve prosthesis with different set ups in order to find what influence geometrical and mechanical characteristics of the aortic conduit have on the valve. These observations will allow to conclude whether or not the introduction of the Valsalva sinuses and the compliance is fundamental in a test bench.

4.2. Materials and methods

4.2.1. Description of test bench

Our test bench aimed at replicating the systemic circulation in compliance with the ISO Standard. The test bench is composed by a reservoir (left atrium), a volumetric pump, a ventricular chamber and adjustable compliance and resistance elements. Both resistance and compliance can be adjusted in order to replicate the physiological pressure curve as close as possible. In the system there are two valve housings: one upstream the ventricular chamber, for the mitral valve where the same polymeric valve will be used throughout testing, and one for the aortic valve, downstream the ventricular chamber, where the valve was changed throughout testing. The pumping system is controlled by a software in which the specific waveform is implemented, and the velocity and stroke volume can be controlled. The pump supplies energy to the service fluid that provokes, through a silicone membrane, the movement of the testing fluid. In the experiment distilled water was used as the service fluid and phosphate buffered saline solution ($\rho = 1000 \text{ kg/m}^3$; $\mu = 0.001 \text{ Pa}\cdot\text{s}$) as testing fluid to preserve the biological valve.

To acquire the required data during the experiments different sensors were used:

- 2 pressure sensors were placed, one 35 mm upstream and one 125 mm downstream the aortic valve;
- 2 flowmeters were alternated, a ½" upstream the valve and a 1" downstream.

The need for two flow sensors arises from the fact that the 1" one does not have a high enough sensibility to register the regurgitant flow correctly while the ½" one has an upper range limit of 20 L/min and cannot register the peak.

4.2.2. Pulsatile test

The pulsatile tests were performed in accordance with the ISO 5840 Standard in physiological conditions. The cardiac frequency used is 70 bpm, the flow rate is approximately 5 L/min and the pressure values, obtained with calibration of the compliance and resistance, were 120 mmHg systolic and 80 mmHg diastolic. The acquisition frequency used is of 200 Hz. For each valve-conduit pair, 3 tests of 25 s were recorded.

In order to easily compare the results, the acquired pressure and flow data were elaborated in a MATLAB code to obtain the different parameters, as required from the Standard [4]. The code firstly read the file and filtered the noise out of the pressure values, then determined the beginning of the systole of each cycle by considering the forward flow. At this point the different parameters indicated in the Standard were calculated for 15 cycles per test and then averaged.

4.2.3. Different types of conduits used

The aim of this thesis was to explore how the geometry and mechanical properties of the set up downstream the aortic valve would affect the valve's performance. To do these three different set ups were tested.

The first set of tests was performed with the standard rigid and straight conduit already present in the original apparatus.



Figure 4.1: Picture of the set up for straight and rigid

Downstream the ventricular chamber there is a 1/2" silicone tube; this tube is connected to an acrylic tube with internal diameter of 34mm and external diameter of 40mm. This tube is inserted into the first part of the valve housing that will be from now on called housing A. On tube 1, 20 mm upstream housing, there is the luer lock for the connection of the upstream pressure sensor. Housing A is tightened to the second one, housing B, with a soft membrane in the middle to act as seal. Housing B is connected to an acrylic tube with the same dimension as the previous one that has, after 125 mm a luer lock is placed to allow connection of the downstream pressure sensor. This tube is then connected through a polymeric block to a 1" silicone tube that leads to the RCR. Tightening happens with two tie rods that go from the polymeric block to housing A and with two additional clamps that hold the housing together.

For the second set of tests, we wanted to have a conduit that was rigid but replicated the geometrical characteristics of the Valsalva sinuses. The cross-section geometry was modeled as an epitrochoid following the equations:

$$x(t) = (R + r) * \cos(t) - \lambda r * \cos\left(\frac{R + r}{r} * t\right)$$

$$y(t) = (R + r) * \sin(t) - \lambda * r * \sin\left(\frac{R + r}{r} * t\right)$$

As a λ value 0.5 was taken since is the one corresponding to normotensive conditions. For the geometrical parameter the following ratios were used [14]:

Table 4.1: Geometric ratios of the aortic root

D_b/D_0	D_a/D_0	L_a/D_0	L_b/D_0	R_{max}/D_0	R_{min}/D_0
1.55	1.25	1	0.34	0.82	0.64

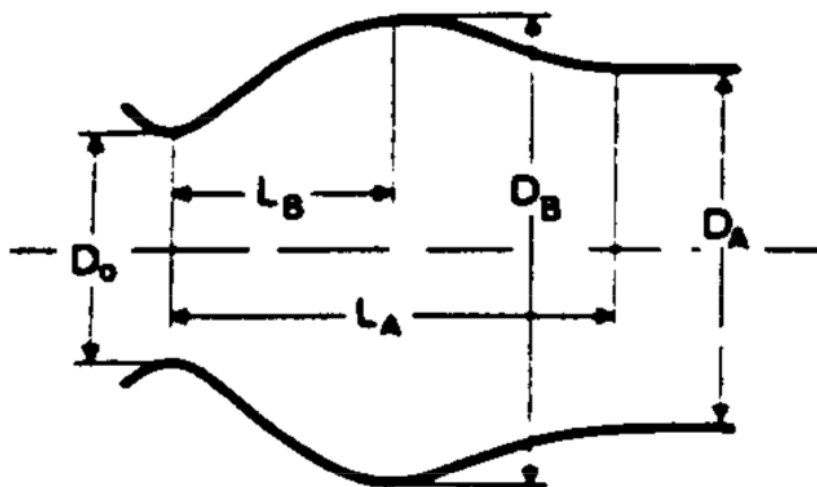


Figure 4.2: Schematic of measurements of the aortic root

Since the values for the exact measures have great variability among the population a value of 34 mm for D_a was chosen to match the internal diameter of the straight tube and all others were extrapolated from it. In the rigid conduit an attachment luer lock was added 75 mm after the Valsalva sinuses in order to insert a pressure sensor when the flow is completely developed. The conduit was designed with a thickness of 3mm.

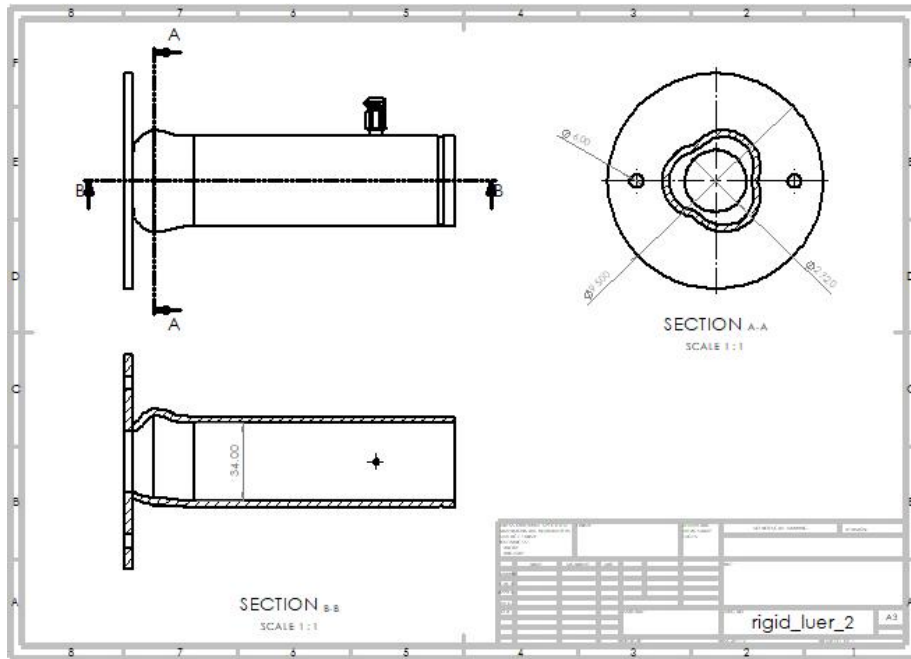


Figure 4.3: CAD model for rigid conduit with Valsalva sinuses

The conduit was designed with SOLIDWORKS and then printed with the Formlabs 3B+ in the clear resin. This resin is a rigid and transparent resin that allowed to create a conduit with virtually no compliance.

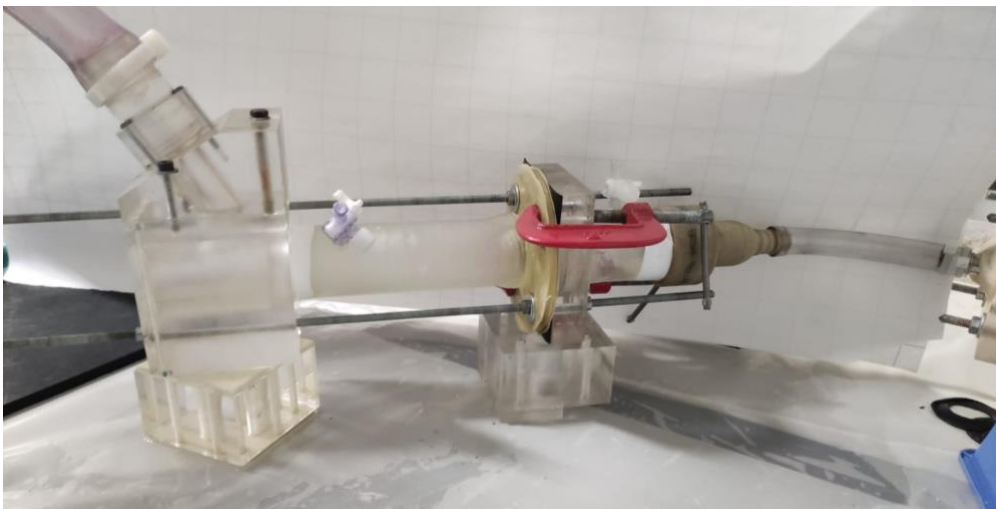


Figure 4.4: Picture of set up for rigid with geometry

The portion of conduit upstream housing A is unaltered, but this part is tightened directly to the rigid conduit that is placed inside the polymeric block. To reduce the risk of damaging the conduit with bolts and clamps a thin and soft silicon membrane was glued to both sides of the plate of the rigid tube. For additional seal a neoprene membrane was cut to shape and placed together with the soft membrane between the housing and the tube. In this case the luer lock was printed directly on the conduit.

For the last set of tests, the compliant tube was printed. The internal geometry is the same used for the rigid one, but the thickness was kept at 1.82 mm. With this thickness the correct compliance will be reached in the 34 mm radius tract while it will be higher in the Valsalva sinuses. This choice was deemed appropriate since the compliance measures used for design were taken in the ascending aorta, downstream the Valsalva sinuses. At the end of the tube an enlargement was placed as to connect it with a standard tube.

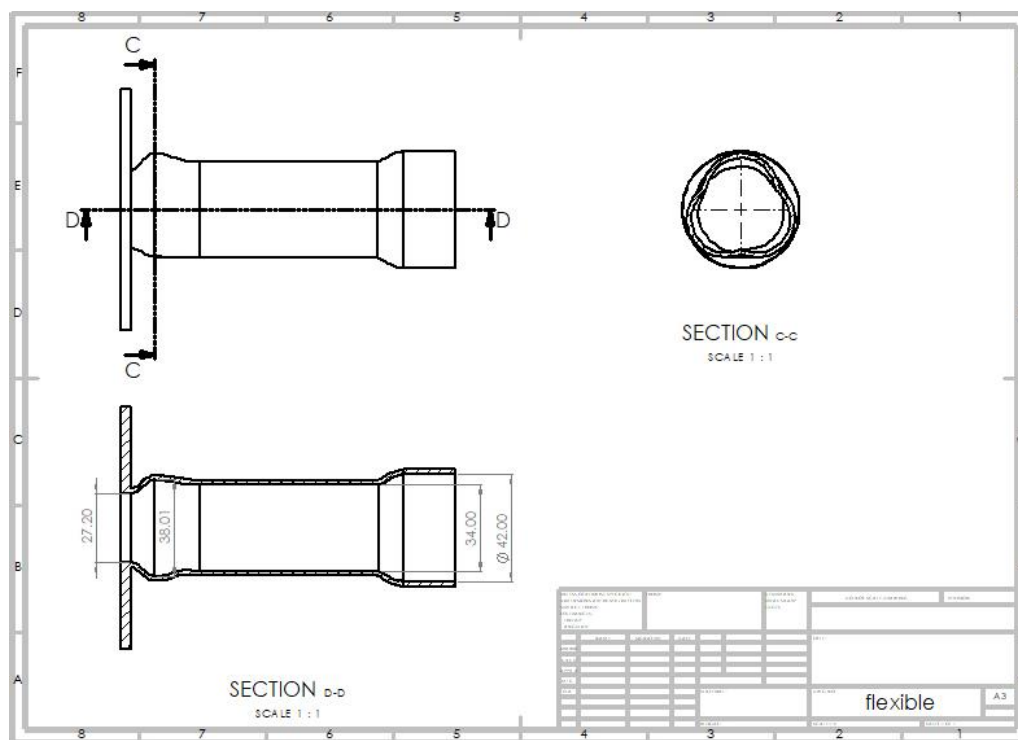


Figure 4.5: CAD model for the compliant conduit

This tube was printed with the Elastic 50A resin previously characterized. A metal plate was used to tighten the tube to the metal housing to avoid leaks.

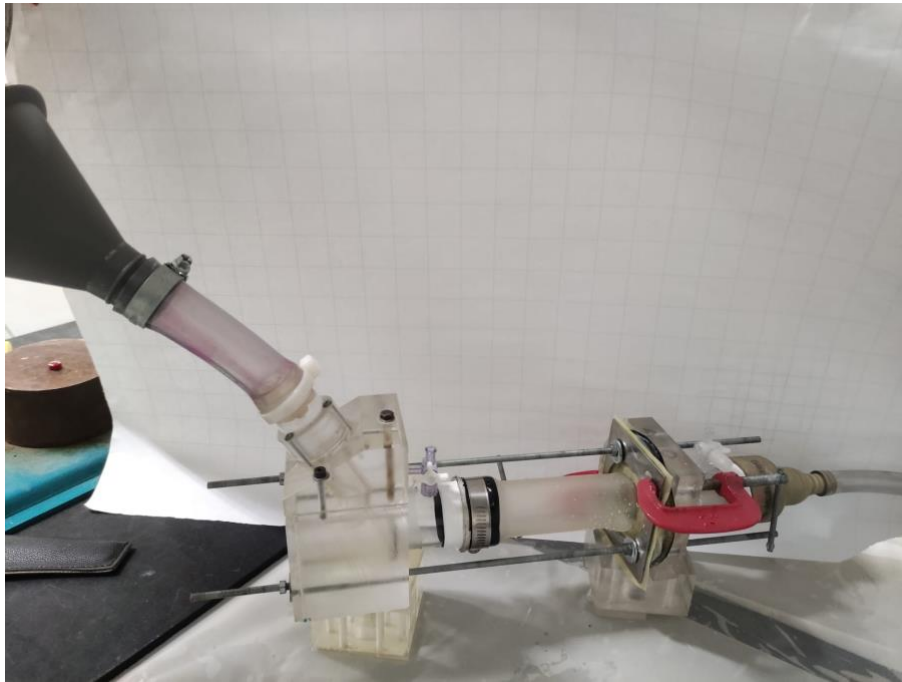


Figure 4.6: Picture of set up for compliant with geometry

Since the plate in this case was not rigid the conduit was tightened to housing A with a metal plate. The sealing action was obtained with the soft membrane and the plate itself that deformed. Since the resin had been observed to have low crack resistance a neoprene membrane was glued to the side of the plate facing the housing while a thin membrane was glued to the other to avoid damages. On the other side of the conduit an acrylic tube that contained the luer lock was connected and secured with a metal strap. The conduit was then inserted in the polymeric block.

4.2.4. Types of valve prosthesis tested

In order to have a complete picture on the different effects on performances, we decided to explore valves with different characteristics and the tests were performed on: a mechanical valve, a biological one and a polymeric one.

For the mechanical valve a bileaflet valve was used, the valve has a 21 mm internal diameter, a 24 mm external one and the leaflets are 12 mm high.



Figure 4.7: Picture of the mechanical valve used for tests

In order to insert it properly in the housing a support was printed in grey resin with the Formlabs 3B+ to contain it.

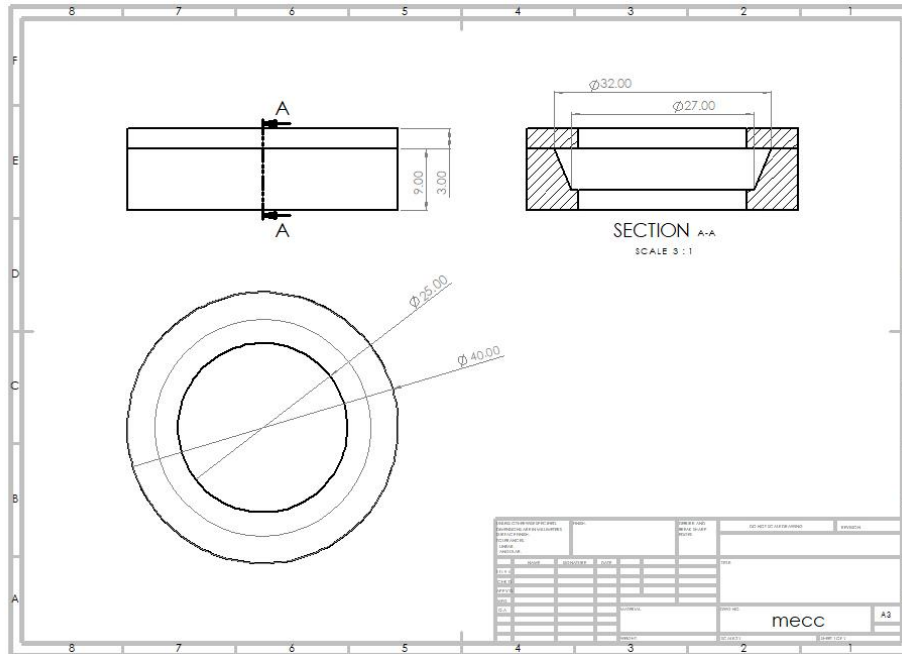


Figure 4.8: Schematic of support for mechanical valve

The biological valve used is the Perimount 3300TFX Magna Ease in the measure 23 mm, with a 22 mm internal diameter, a 26 mm external one and 12mm of leaflets height.

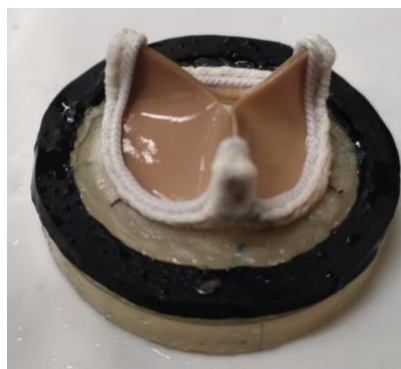


Figure 4.9: Biological valve used for tests

This valve was sutured to its support using nylon thread; silicone was used to close the gap between the valve and the support, and two polymeric seals were then placed on top of it to block it completely.

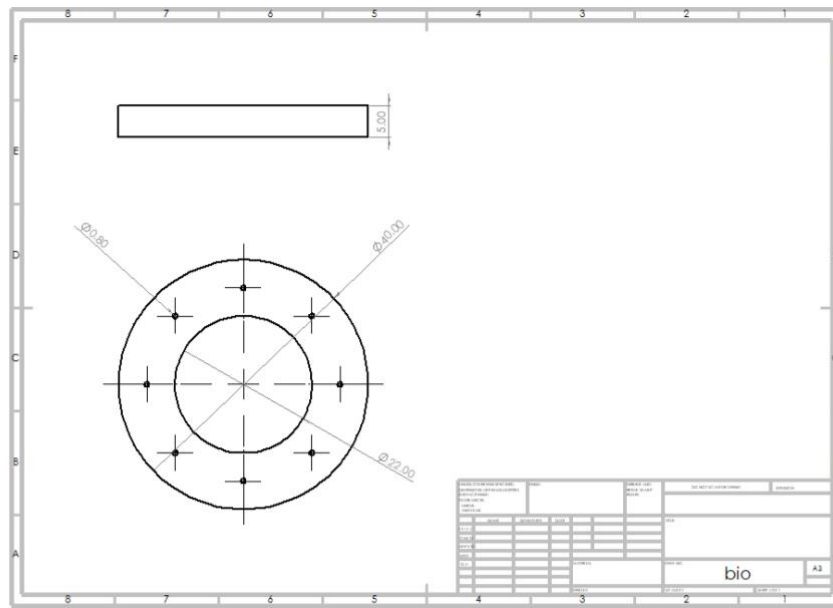


Figure 4.10: Schematic of support for biological valve

As a polymeric valve a Poli-Valve, a polymeric valve developed by the Politecnico di Milano in collaboration with Cambridge University and not available on the market was used. The valve is made of a styrene block copolymer and has a 20 mm internal diameter, a 25 mm external one and 12 mm of leaflet height [10]. Since this valve had already been used in this test bench it was already contained in a custom-made support.



Figure 4.11: Polymeric valve used for tests

4.3. Results

From the extracted data the following will be considered in detail: the mean pressure drop caused by the valve, the root mean square of the instantaneous flow rate (Q_{RMS}) representing the forward flow, the effective orifice area calculated for the valve and the percentage of regurgitant flow. In the graph the theoretical behavior of aortic flowrate, upstream and downstream pressure is shown [27].

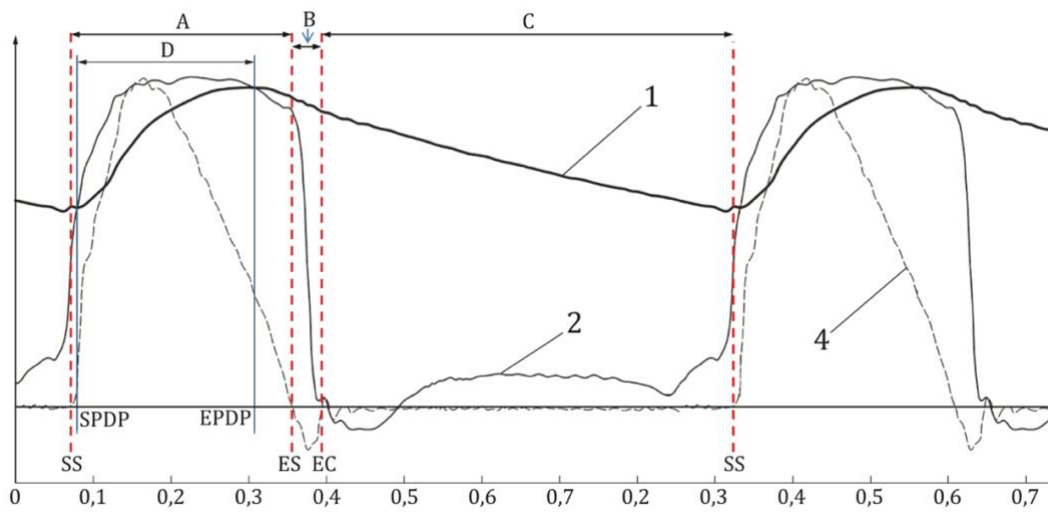


Figure 4.12: Downstream pressure (1), Upstream pressure (2) and aortic flowrate (4) during a cycle

The mean pressure difference (MPD) was calculated as:

$$MPD = \frac{\sum_{i=1}^n \Delta P_i}{n}$$

Where n is the number of samples during which ΔP_i , the pressure difference, in mmHg, across the valve, is positive. The MPD will be the average over the positive differential pressure period, SPDP to EPDP or zone D, of the difference between 2 and 1.

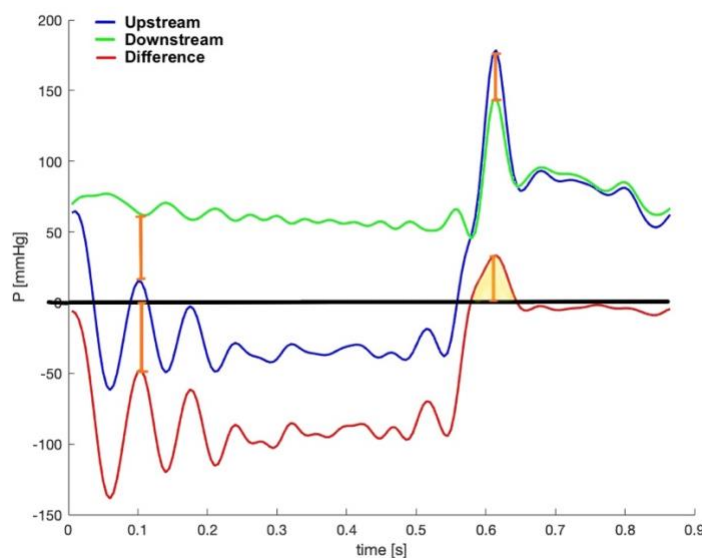


Figure 4.13: Example of calculation of pressure difference (red) starting from upstream (blue) and downstream (green) pressure

In figure 4.13 the pressure drop is shown during the whole cycle; the shaded area is the positive differential pressure period.

Q_{RMS} , the root mean square of the forward flow, in milliliter per second, was given by:

$$Q_{RMS} = \sqrt{\frac{\int_{t_1}^{t_2} Q(t)^2 dt}{t_2 - t_1}}$$

With $Q(t)$ being the instantaneous flow and t_1 and t_2 marking the beginning and end of positive differential pressure period, zone D in figure 4.12. This region, and not the positive flow region A, is used for the calculation of Q_{RMS} in order to provide consistent values of EOA for comparison with the minimal requirements [28].

The effective orifice area (EOA) was calculated as:

$$EOA = \frac{Q_{RMS}}{51.6 * \sqrt{\frac{\Delta P}{\rho}}}$$

Where the density ρ was taken to be 1 g/cm³ for phosphate buffered saline solution and ΔP is the MPD.

Regurgitation Volume is calculated as:

$$RG = \int_{t_3}^{t_4} Q(t) dt$$

Where t_3 and t_4 are the start and end time of the backflow, corresponding to end and beginning of systole [27]. The percentage of regurgitant flow is then calculated as:

$$Reg\% = \frac{RG}{SV} * 100$$

Where SV is the stroke volume, the volume of fluid pushed forward during systole.

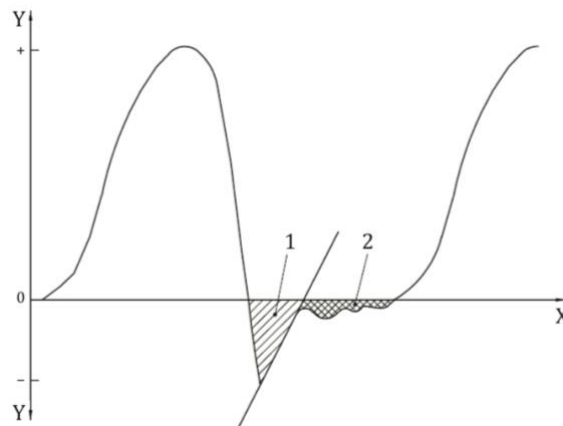


Figure 4.14: Graph showing flowrate vs time in cycle as given in the Standard

In figure 4.14 is clearly shown the separation between closing volume (1) and leakage volume; conventionally leakage starts when the negative flow reaches for the first time a certain value, in this work assumed to be 40 mL/min, and lasts until the start of systole [28].

In addition to the indexes, a graphic comparison is shown for flow, regurgitant flow, upstream and downstream pressure.

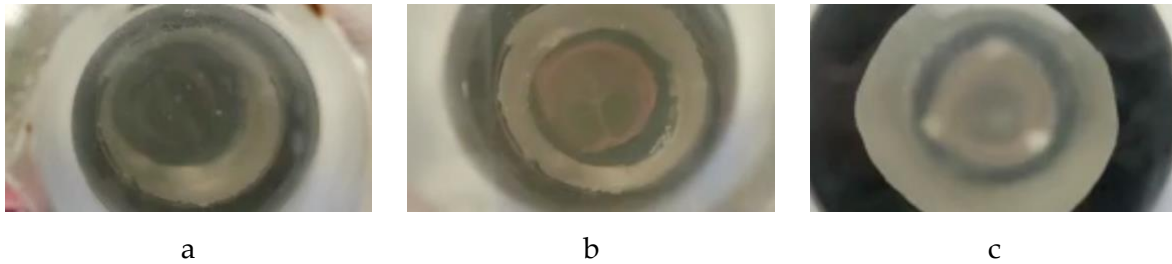


Figure 4.15: Videos showing the mechanical (a), polymeric (b), and biological (c) heart valve prostheses

Mean Pressure Difference

In the following table the average results obtained for MPD are shown.

Table 4.2: MPD results for each of the tested conditions

MPD (mmHg)	Mechanical	Polymeric	Biological
Standard	24.0 ± 2.7	15.7 ± 3.2	21.8 ± 7.1
Valsalva sinuses rigid	89.6 ± 3.0	11.7 ± 2.3	17.0 ± 2.4
Valsalva sinuses compliant	26.5 ± 3.5	16.0 ± 1.4	13.6 ± 1.7

The introduction of the Valsalva sinuses reduces the pressure drop in the polymeric and biological valve while there is a clear increase shown for the mechanical valve. The reason for this can be searched in the different designs of the valves: the mechanical valve is a bileaflet valve while the other two are trileaflet. Since the sinuses have three lobes the leaflets of the trileaflet valves fit naturally in them, as a result the opening of the valve is aided by this structure and the pressure drop is reduced. With the bileaflet instead the fluid dynamics generated by the valve do not match the ones generated by the sinuses and the pressure increases significantly [29].

When the compliance is introduced, the pressure drop and fluid dynamics discontinuities are distributed along the tube so the mismatch observed for the mechanical valve is reduced and the pressure drop decreases. Since the pressure difference peak is distributed over a larger time the average results lower as shown for

the biological valve. The unexpected behaviour of the polymeric valve can be justified considering the graph for the rigid with Valsalva sinuses configuration.

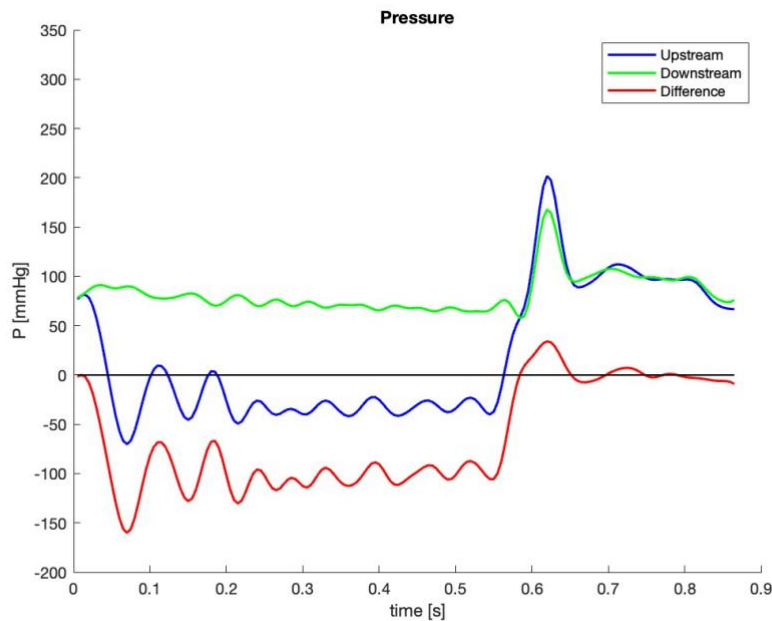


Figure 4.16: Upstream, downstream, and differential pressure for the polymeric valve in the rigid configurations

In fact, we can see not one but two regions with positive differential pressure; the second one is not present for the biological valve and disappears for the polymeric with the compliant tube. Since the second region has a low intensity spread over a large time interval it will decrease the MPD value significantly. With this configuration the differences shown by the polymeric valve in the different configuration are small compared to the ones for the biological one; this could be due to the fact that the polymeric valve is more rigid so its pressure drop may be less affected by the conduit behaviour.

Flowrate index

The system works with a volumetric pump, so the forward flow should not feel much the difference in set up. In particular if we consider the compliant conduit the forward flow at the first cycle would likely be reduced due to sequestered fluid but, at the next cycle, this extra fluid is pumped forward while more is sequestered. In conclusion the overall behaviour after the transitory is unaltered. This is confirmed by the results for the stroke volume that are unaltered in all configurations.

Table 4.3: SV results for each of the tested conditions

SV (ml)	Mechanical	Polymeric	Biological
Standard	65.5 ± 0.3	66.2 ± 0.3	66.3 ± 0.4
Valsalva sinuses rigid	67.4 ± 0.4	66.0 ± 0.4	66.1 ± 0.4
Valsalva sinuses compliant	66.1 ± 0.4	65.4 ± 0.5	65.3 ± 1.0

For Q_{RMS} instead only the flow during the positive differential period is considered. The changes seen can then be justified with variation of this time period. For the mechanical valve, as shown in figure 4.17, in standard configuration the time is shorter that in the other two configurations, it is significantly increased with the Valsalva sinuses and slightly increased with the compliance.

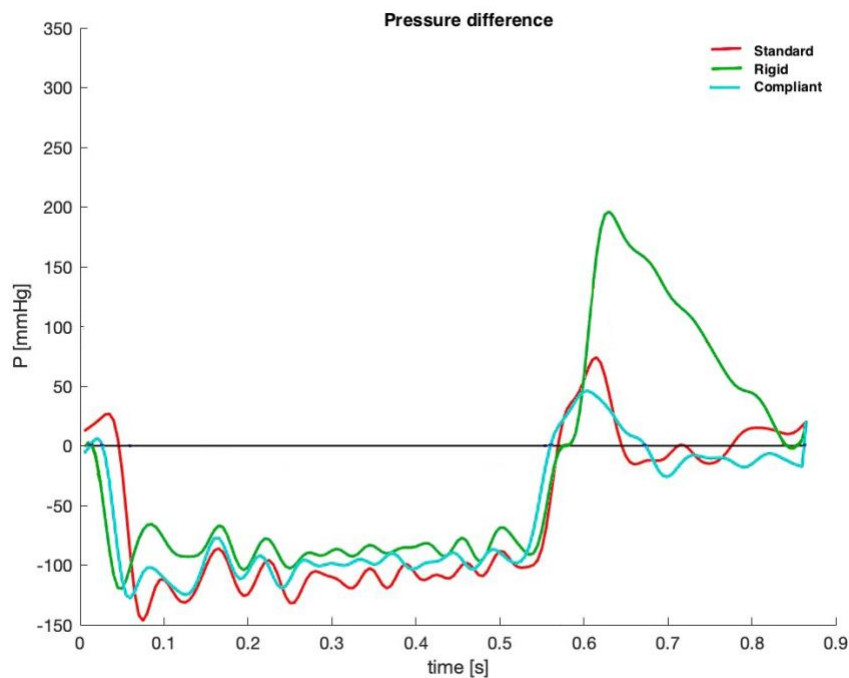


Figure 4.17: Pressure difference for the mechanical valve in the three different configurations

Similarly, the positive differential period is longer for the polymeric and biological valve in the compliant configuration. The second region seen for the polymeric valve in the rigid configuration is not significant for this calculation since at that time the flow has already decreased significantly.

Table 4.4: Q_{RMS} results for each of the tested conditions

Q_{RMS} (ml/s)	Mechanical	Polymeric	Biological
Standard	12.0 ± 1.0	16.2 ± 1.2	15.8 ± 1.9
Valsalva sinuses rigid	16.6 ± 0.2	16.1 ± 0.8	14.6 ± 0.9
Valsalva sinuses compliant	14.2 ± 1.4	12.0 ± 1.4	12.6 ± 1.7

Effective Orifice Area

In the following table the average results obtained for EOA are shown.

Table 4.5: EOA results for each of the tested conditions

EOA (cm ²)	Mechanical	Polymeric	Biological
Standard	0.8 ± 0.1	1.4 ± 0.2	1.1 ± 0.2
Valsalva sinuses rigid	0.6 ± 0.0	1.6 ± 0.2	1.2 ± 0.1
Valsalva sinuses compliant	0.9 ± 0.1	1.0 ± 0.1	1.1 ± 0.2

As expected from the definition of effective orifice area the changes are related to the behaviour of MPD and Q_{RMS} . It is interesting to consider the requirements for EOA values according to size here listed [4].

Table 4.6: Requirements for EOA as listed in the Standard

Valve size (mm)	17	19	21	23	25	27	29	31
EOA (cm ²)	0.70	0.85	1.05	1.25	1.44	1.70	1.95	2.25

All the prosthesis tested are around a size 21 and the minimum requirement is to have a 1.05 cm² EOA. Comparing this value with the ones shown in table 4.5 we can conclude that the polymeric and biological valve would have passed in all conditions even if the configuration in the Valsalva sinuses improves the performances of both. The mechanical one is too stenotic in all set ups. The mechanical valve was expected to be more stenotic than the others due to a different opening mechanisms that leaves a smaller orifice open.

Regurgitation percentage

In the following table the average results obtained for the regurgitation percentage are shown.

Table 4.7: Regurgitation results for each of the tested conditions

Regurgitation %	Mechanical	Polymeric	Biological
Standard	14.5 ± 1.3	6.5 ± 0.2	12.6 ± 0.4
Valsalva sinuses rigid	8.6 ± 0.6	5.9 ± 0.2	14.3 ± 0.1
Valsalva sinuses compliant	19.8 ± 0.7	7.0 ± 0.2	17.6 ± 0.3

The introduction of Valsalva sinuses is believed to lead to the formation of vortexes that aid the closure of the valve; this claim is supported by the shown decrease in regurgitation. The only exception is the biological valve where the trend is inverted; this could possibly not be related to the valve itself but to how it was supported. In fact, out of the three valves the biological one had the least precisely fitted support and paravalvular leakage was observed in a static test. If then the regurgitation for this valve is mostly paravalvular then the introduction of vortexes would worsen the performance since more flux passes around the valve. In addition to this consideration the biological valve has an external diameter of 26 mm, the highest of the valves tested. It is possible that this large dimension, only 1 mm smaller than the diameter upstream the sinuses, makes it so that the effect of the sinuses is felt less by the leaflet thus not bringing the same beneficial effect observed in the other valves.

When compliance is introduced, the regurgitation increases for all tested valves. In its natural role the compliance of the vessel should allow it to expand during systole and recoil during diastole; this recoil pushes the blood into the coronaries that originate in the Valsalva sinuses. Since in our configuration the Valsalva sinuses are not replicated the fluid pushed during recoil has no low resistance path, part of it will be pushed forward but a portion will be pushed back during the valve. Since the recoil of the tube will start at the end of the positive differential period, the valve is not fully closed yet and the regurgitation, especially during closure is increased.

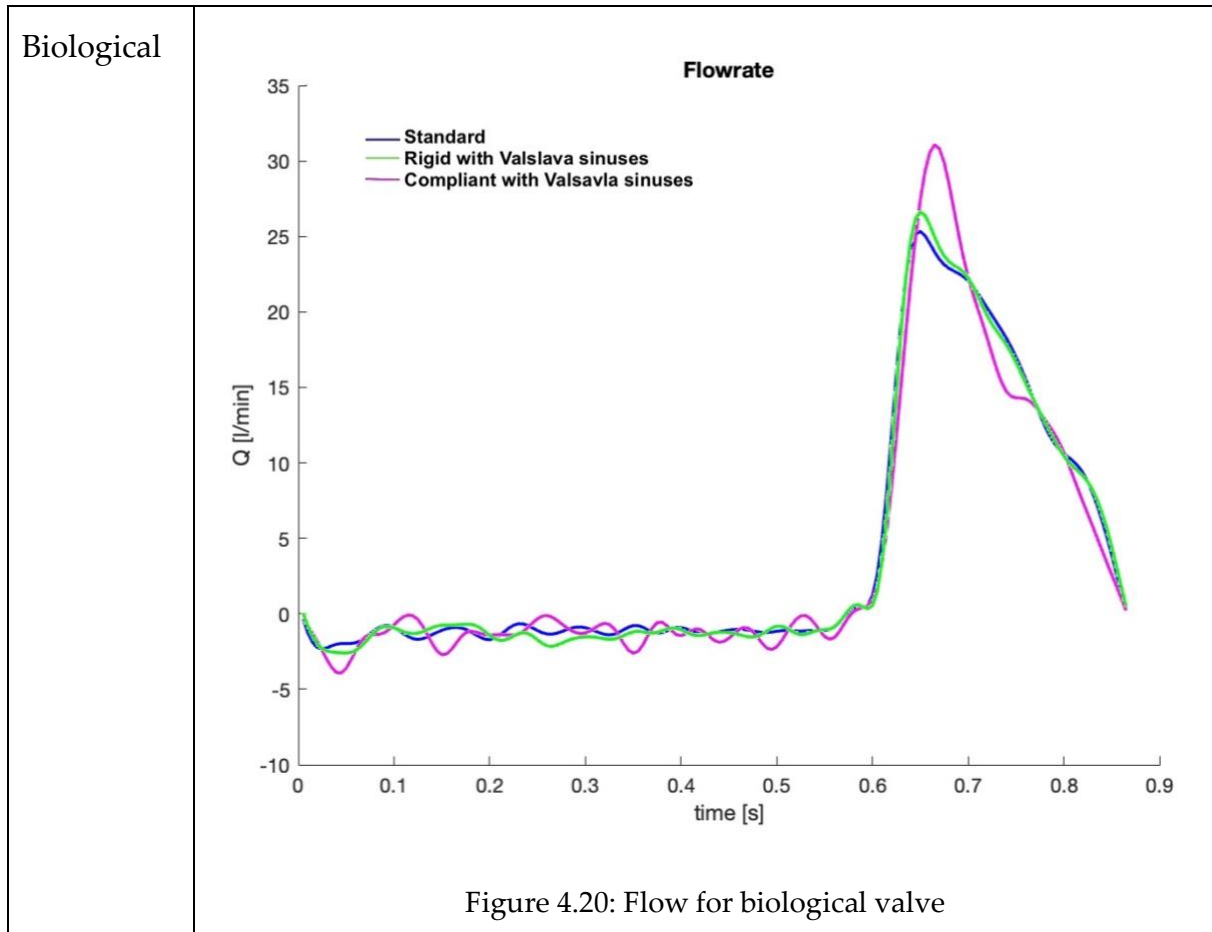
According to the standard the maximum regurgitation percentage acceptable is 10% [28]. Following that the only valve to not result insufficient would be the polymeric. It should be noted that the tests are performed with saline solution, not blood. When blood is used coagulation happens around the Dacron ring, decreasing the paravalvular leakage very likely present in both mechanical and biological valve.

Graphs for flow rate

The following graphs represent the flow rate measured with the 1" sensor during one cycle in each condition.

Table 4.8: Flow behavior for a sample cycle in each testing condition for each valve

<p>Mechanical</p>	<p>The graph shows flow rate (Q) in l/min on the y-axis (ranging from -10 to 35) against time in seconds (s) on the x-axis (ranging from 0 to 0.9). Three data series are plotted: Standard (blue), Rigid with Valsava sinuses (green), and Compliant with Valsava sinuses (magenta). All series show a sharp increase in flow rate starting around 0.6s, peaking at approximately 0.65s. The 'Compliant with Valsava sinuses' condition reaches the highest peak of about 31 l/min, while the 'Standard' condition peaks at about 25 l/min. The 'Rigid with Valsava sinuses' condition peaks at about 24 l/min. All series show a gradual decrease in flow rate after the peak, returning to near zero by 0.85s.</p>
<p>Figure 4.18: Flow for mechanical valve</p>	
<p>Polymeric</p>	<p>The graph shows flow rate (Q) in l/min on the y-axis (ranging from -10 to 35) against time in seconds (s) on the x-axis (ranging from 0 to 0.9). Three data series are plotted: Standard (blue), Rigid with Valsava sinuses (green), and Compliant with Valsava sinuses (magenta). All series show a sharp increase in flow rate starting around 0.6s, peaking at approximately 0.65s. The 'Compliant with Valsava sinuses' condition reaches the highest peak of about 31 l/min, while the 'Standard' condition peaks at about 26 l/min. The 'Rigid with Valsava sinuses' condition peaks at about 25 l/min. All series show a gradual decrease in flow rate after the peak, returning to near zero by 0.85s.</p>
<p>Figure 4.19: Flow for polymeric valve</p>	

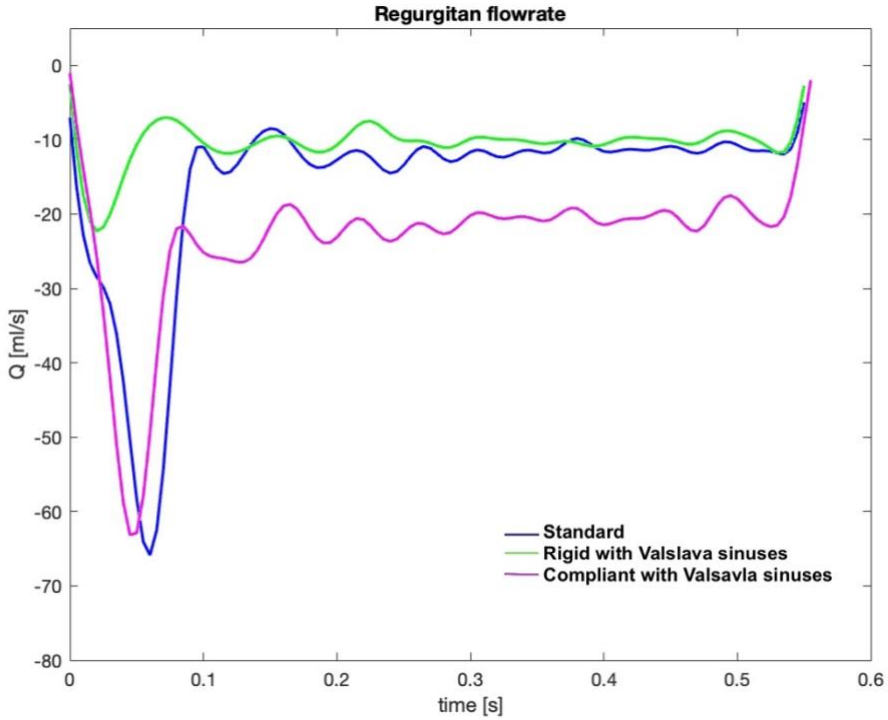
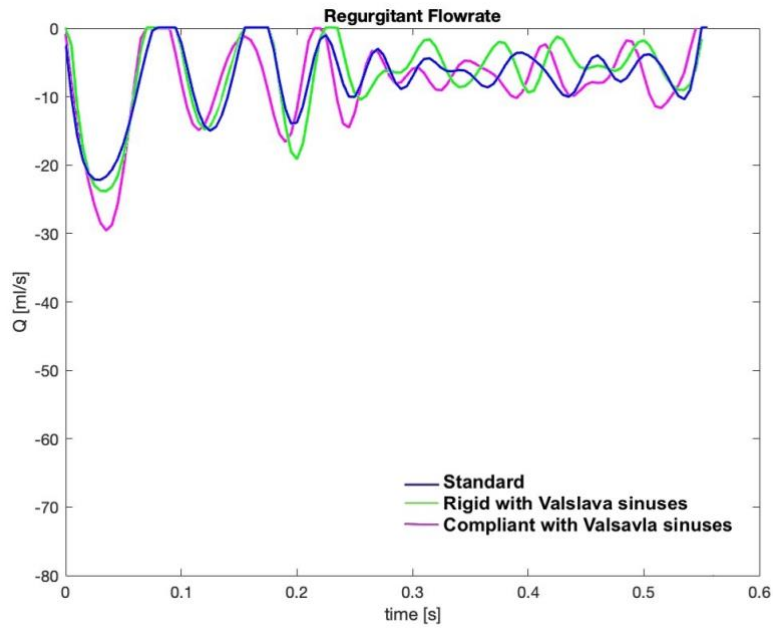


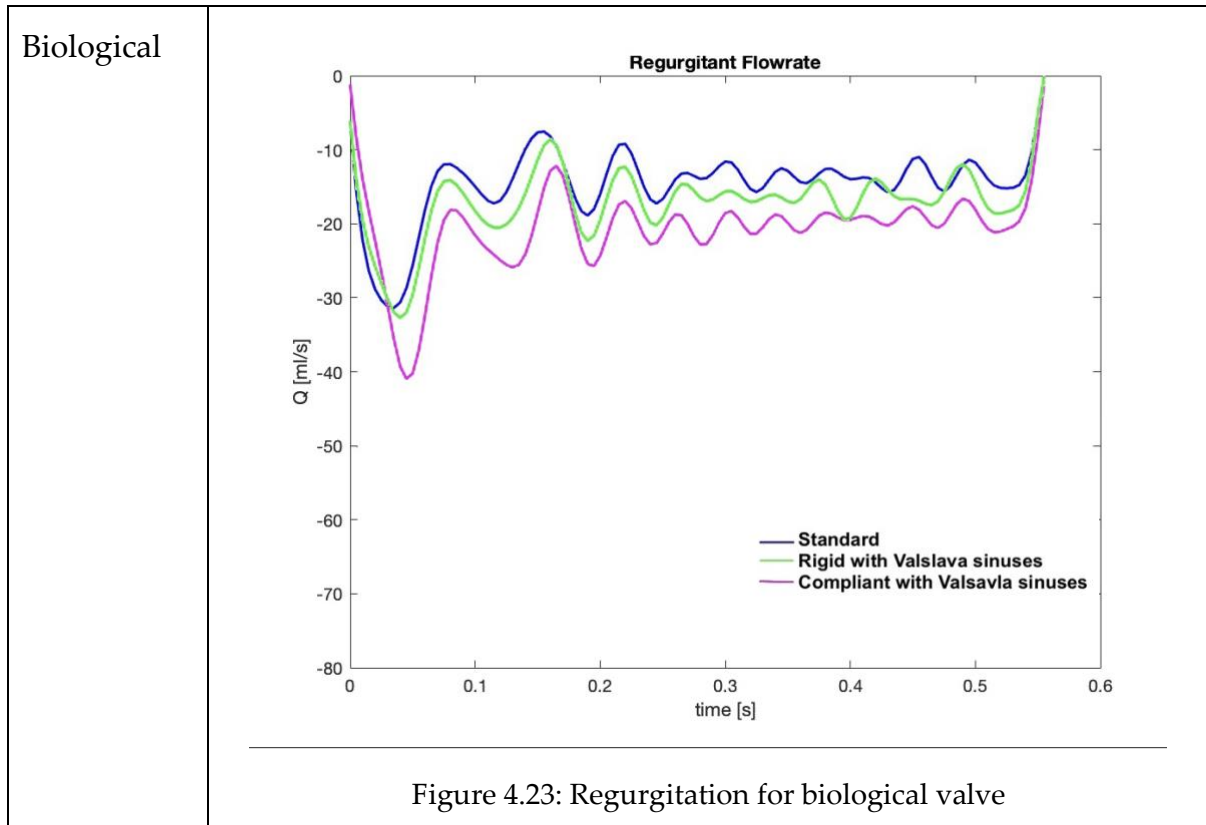
The introduction of the Valsalva sinuses does not influence much the flow peak. Instead, the compliance makes the peak higher, passing from around 25 L/min to more than 30 L/min. The compliant conduit expands when the valve opens, pushed by the flow, this allows a larger volume of water to pass initially since it encounters a reduced resistance if compared to the one of the rest of the circuit. As seen before however the total stroke volume is unaffected. The compliance then affects the instantaneous flow that is 20% higher when the valve opens but decreases more rapidly than in the other configurations.

Graphs for regurgitant flow

The following graphs represent the regurgitant flow measured with the 1/2" sensor during one cycle in each condition.

Table 4.9: Regurgitant flow behavior for a sample cycle in each testing condition for each valve

Mechanical	 <p style="text-align: center;">Figure 4.21: Regurgitation for mechanical valve</p>
Polymeric	 <p style="text-align: center;">Figure 4.22: Regurgitation for polymeric valve</p>



As shown before in table 4.6, the presence of Valsalva sinuses reduced the regurgitation percentage; in the graphs in table 4.9 is visible, however, how this reduction is not distributed in the same way during diastole. The mechanical valve shuts faster in this configuration and, thanks to its rigidity, once closed the leaflets are stable; this leads to a reduction in both closing and leakage volume. In the polymeric and biological valve instead, no significant difference can be appreciated in the leakage while closing volume decreases. Numerical values for closing and leaking volume are shown in table 4.11. The vortices may have less effect on the trileaflet valves, as we saw in the MSPD section, during the closing phase, leaving the closing volume basically unchanged. Regarding leaking volume, it is decreased in the polymeric valve while increases in the biological one, keeping the same oscillation but at lower values; as stated when talking about regurgitation volume in general these lower values could indicate a negative flow pushed around the valve, not through it. The introduction of a compliant conduit leads to a higher volume being pushed back during valve closure due to the recoil of the conduit. As a result, we see a downwards shift of the graph resulting in higher leakage and closing volume especially for the biological and mechanical valves, more affected by paravalvular leakage. The polymeric valve seems to be less affected than the others; this could be due to a combination of the trileaflet geometry, designed to better suit the physiology, more rigid leaflets, more stable and a perfectly matching housing with low to null paravalvular leakage.

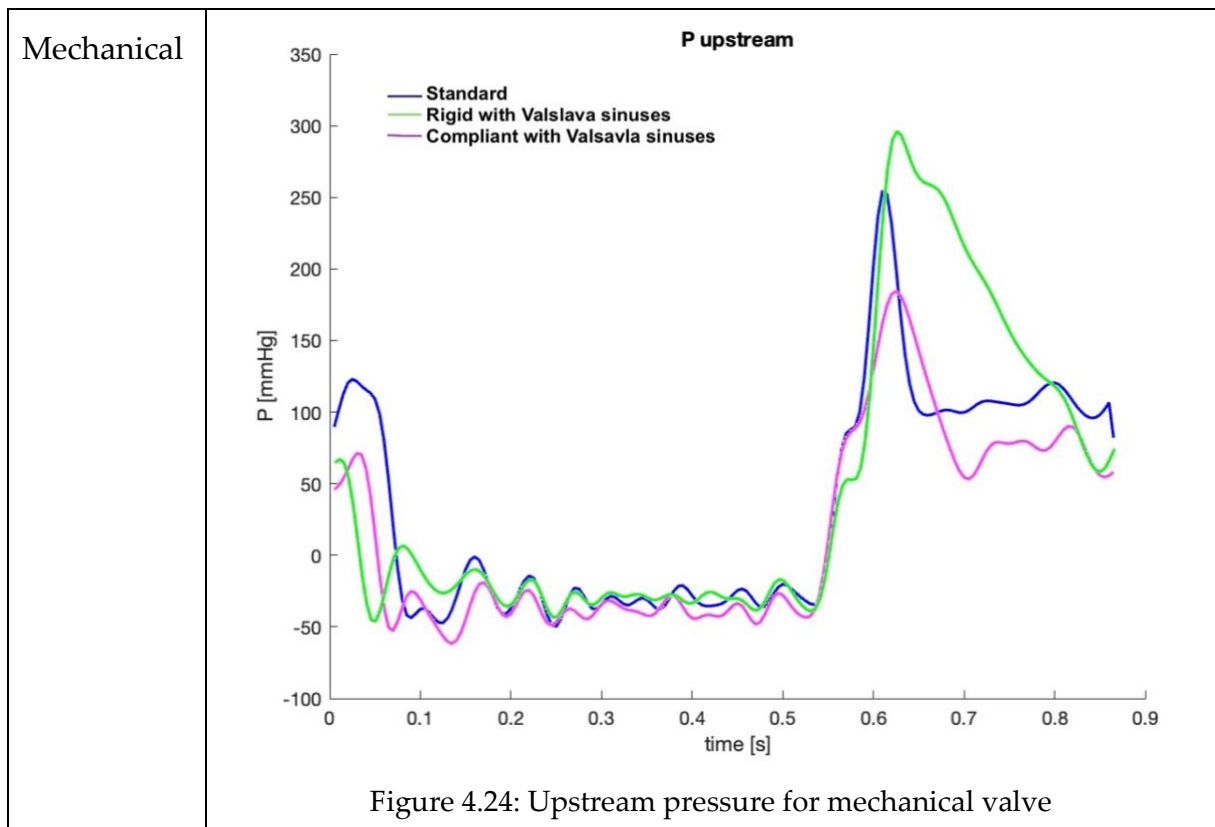
Table 4.10: Results for closing and leakage volume for each condition

V (mL)	Mechanical		Polymeric		Biological	
	closing	leakage	closing	leakage	closing	leakage
Standard	5.1	4.4	1.9	2.3	3.5	4.9
Valsalva sinuses rigid	2.3	3.5	1.8	2.0	3.8	5.7
Valsalva sinuses compliant	5.7	7.4	2.2	2.4	6.9	17.6

Graphs for upstream pressure

The following graphs represent the pressure measured upstream the valve during one cycle in each condition.

Table 4.11: Upstream pressure behavior for a sample cycle in each testing condition for each valve



Polymeric

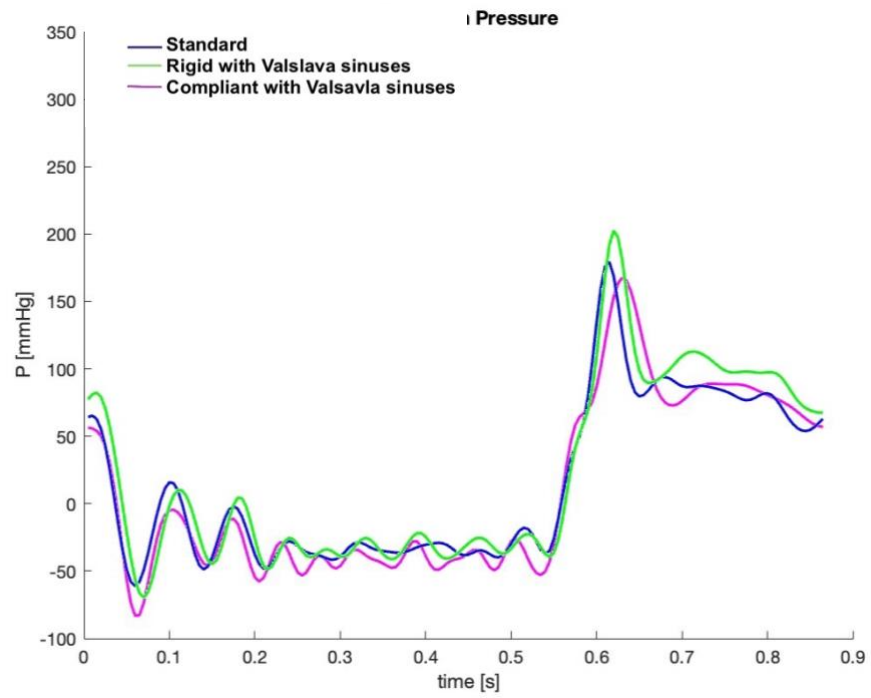


Figure 4.25: Upstream pressure for polymeric valve

Biological

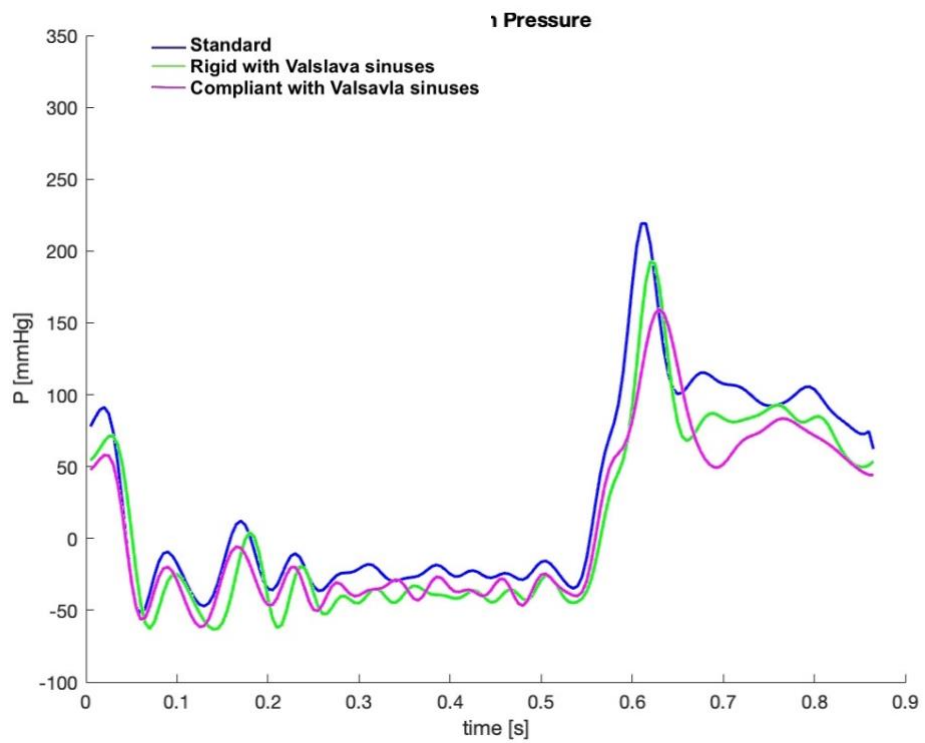


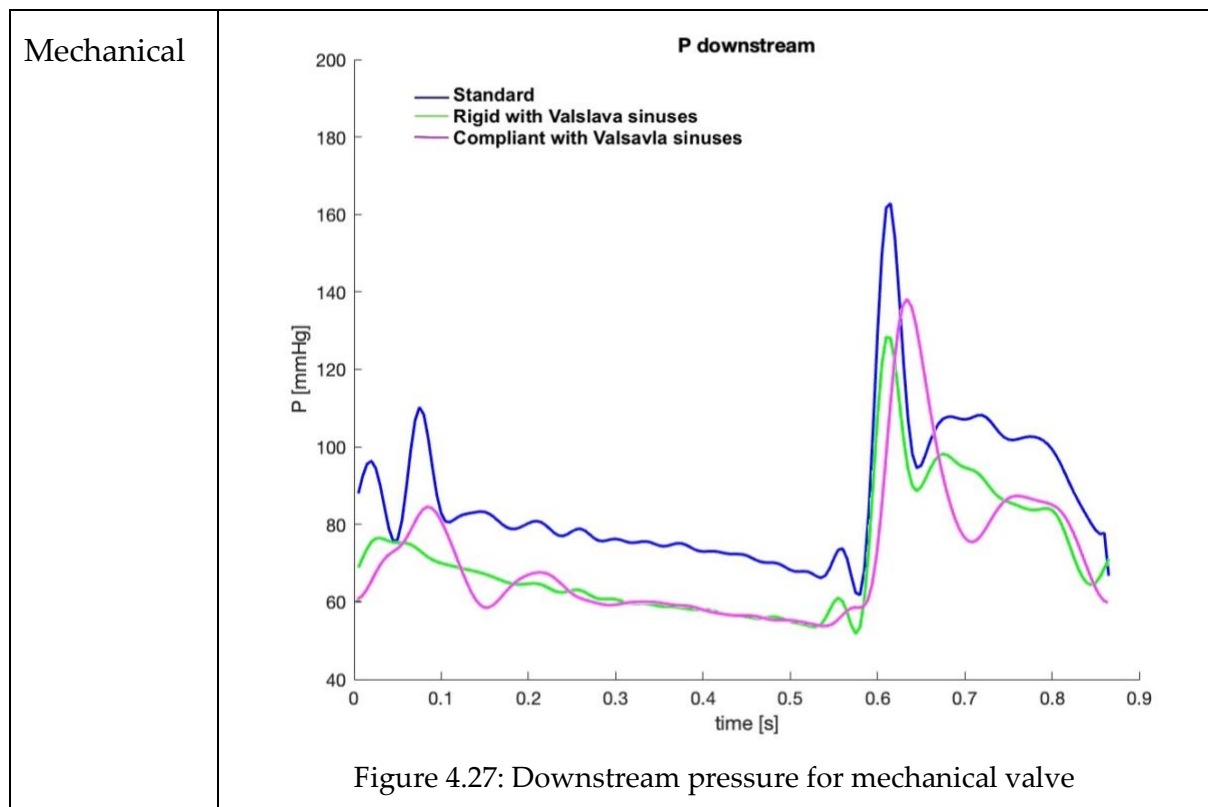
Figure 4.26: Upstream pressure for biological valve

The introduction of Valsalva sinuses determines an increase in the peak of upstream pressure, especially evident for the mechanical valve, due to the diameter reduction; this increase is not observed for the biological valve since its larger size makes it less affected by the reduction. The diastolic phase appears unaffected. With the compliant conduit we see a general reduction of pressure, possibly because the less rigid conduit reduces the effect of the diameter reduction. Moreover the whole pressure curve is smoothed due to the effect of the compliance that tends to mitigate pressure variations.

Graphs for downstream pressure

The following graphs represent the pressure measured downstream the valve during one cycle in each condition.

Table 4.12: Downstream pressure behavior for a sample cycle in each testing condition for each valve



Polymeric

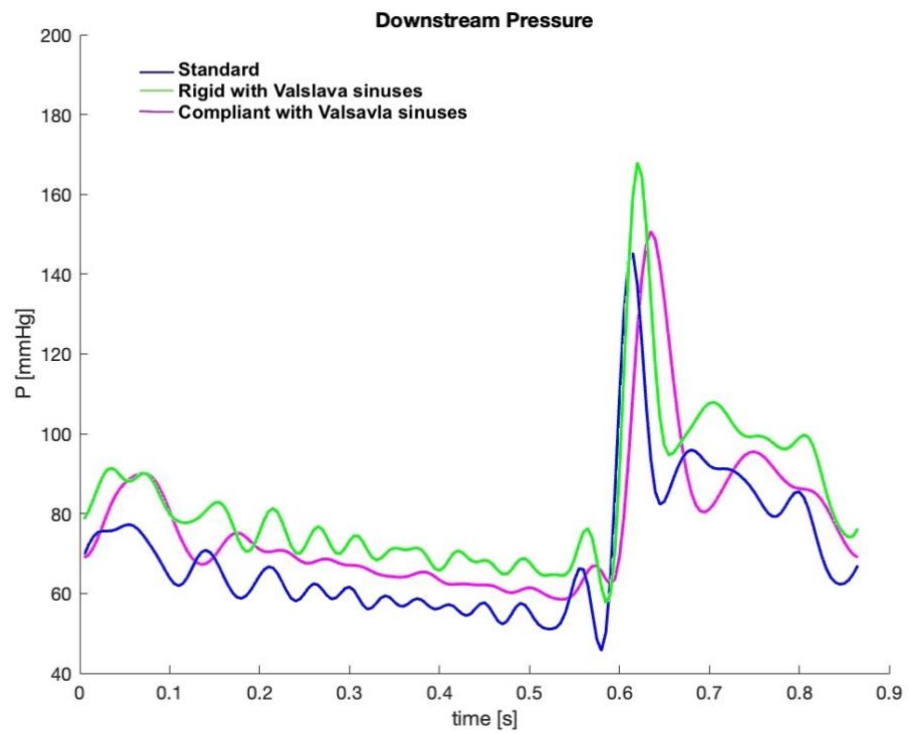


Figure 4.28: Downstream pressure for polymeric valve

Biological

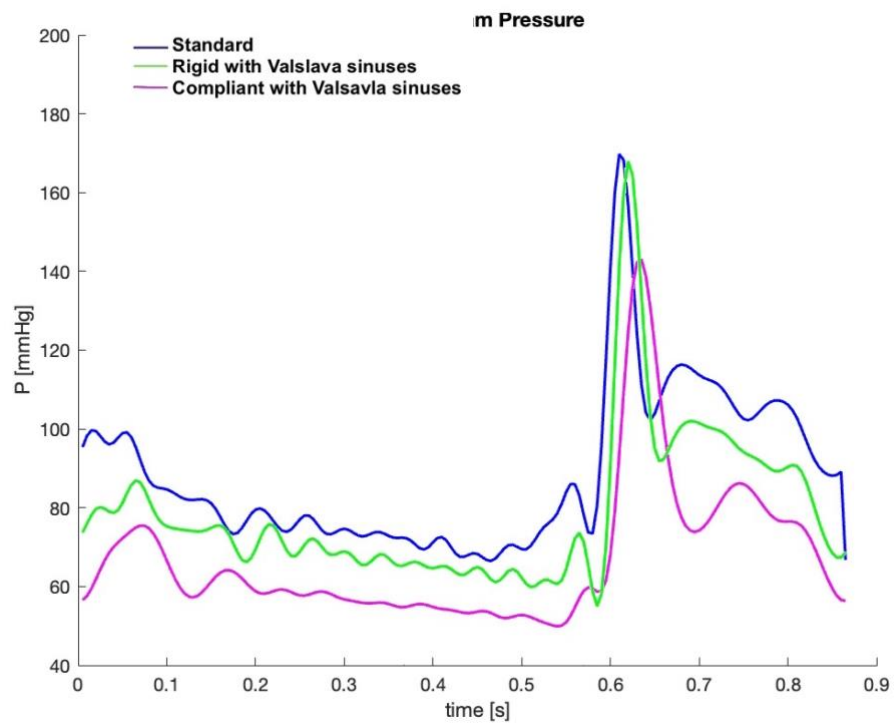


Figure 4.29: Downstream pressure for biological valve

The peak of the downstream pressure was supposed to be kept at the same level by adjusting resistances in every experiment, oscillations in its intensity are to be considered as experimental error. It is significant, however, to note that the peak in the compliant configuration is delayed; this happens because the sensor for downstream pressure was placed downstream the compliant conduit that affects the pressure variation.

Conclusion and future developments

In this work we have shown that it is possible to exploit 3D printing to obtain an aortic phantom with physiological mechanical and geometrical characteristics and use it to perform pulsatile tests on aortic valve prosthesis. Moreover, we show how to obtain the required parameters and produce the conduit using the Formlabs 50A resin.

We have seen how the introduction of Valsalva sinuses had different effects on the pressure drop of different valve types; moreover, the differences shown by trileaflet vs bileaflet valves underline how the use of a physiologically shaped valve is a significant advantage but only if the prosthesis is placed appropriately. The increased regurgitation has been correlated with a vortex formation that should be confirmed by performing some tests to show the fluid dynamics; an example of this tests is particle image velocimetry that would allow to directly visualize the flow.

The introduction of compliance brought significant differences in the parameters considered but, especially regarding the regurgitation results, it is essential to perform new tests in which the coronaries are taken into account in order to better study the effect of the compliance on the valve's performances. It is also possible that in this case having a concentrated systemic impedance might affect the performance of the conduit if compared with the distributed situation in vivo. Since a set up with a distributed impedance would be definitely challenging it could be interesting to perform in silico tests on the differences given on a compliant tube by a concentrated vs distributed impedance.

Lastly, we can consider that a measure of error may be introduced by the valve supports; as an improvement the housing could be redesigned so to block a soft structure onto which the valve would be sutured thus reproducing the same level of paravalvular leakage that could be experienced during service of the sutured prosthesis; moreover, more accurate results would be obtained using blood.

In this work we have shown how much the geometrical and mechanical characteristics of the conduit downstream the aortic valve affect its performances. The Standard enforces minimum performance requirements but considering the level of freedom that leaves on the set up each manufacturer could find the conditions that lead to better performances of its valve and only present those results. This results in a lack of uniformity that should be the primary scope of the Standard. It is than of cardinal importance to develop a unified testing system that takes physiological conditions into account to allow a meaningful comparison of valve performances. According to the results here presented it would seem that having a conduit with Valsalva sinuses could bring the in vitro test one step closer to the physiological situation by introducing a more similar fluid dynamic configuration. Regarding the compliance instead the results were not as promising since the performances of the valves were heavily

affected by some set up limitations. After additional studies adding also the compliance should be considered.

Bibliography

- [1] A. Pick, «HeartValveSurgery.com,» [Online]. Available: <https://www.heart-valve-surgery.com/heart-valve-replacement.php>.
- [2] S. Rizzi, S. Ragazzini e M. Pesce, «Engineering Efforts to Refine Compatibility and Duration of Aortic Valve Replacements: An Overview of Previous Expectations and New Promises,» *Frontiers in Cardiovascular Medicine*, vol. 9, 2022.
- [3] S. Marconi, E. Lanzarone, G. H. Van Bogerijen, M. Conti, F. Secchi, S. Trimarchi e F. Auricchio, «A compliant aortic model for in vitro simulations: Design and manufacturing process,» *Medical Engineering and Physics*, vol. 59, pp. 21-29, 2018.
- [4] B. S. Institution, «Cardiovascular implants. Cardiac valve prostheses. Part 2, Surgically implanted heart valve substitutes,» 2021.
- [5] G. Comunale, L. Di Micco, D. P. Boso, F. M. Susin e P. Peruzzo, «Numerical models can assist choice of an aortic phantom for in vitro testing,» *Bioengineering*, vol. 8, n. 8, 2021.
- [6] R. Barone, V. Benagiano, F. Bucchieri, C. Campanella, F. Cappello, F. Carini, G. A. Cavalletti, M. G. Cusella De Angelis, V. D'agata, S. David, A. De Luca, V. Di Felice, G. G. A. Gobbi, V. Grill, G. Guerra, M. Gulisano, V. Macchi e M, *Anatomia Umana, basi anatomiche per la fisiologia*, Edises Università.
- [7] M. S. Sacks e A. P. Yoganathan, «Heart valve function: A biomechanical perspective,» *Philosophical Transactions of the Royal Society B: Biological Sciences*, vol. 362, n. 1484.
- [8] R. B. Hinton e K. E. Yutzey, «Heart valve structure and function in development and disease,» *Annual Review of Physiology*, 2011.
- [9] D. Harkem, «Heart Valves: ten commandments and still counting,» *Annals of thoracic surgery*, vol. 48, n. 3, 1989.

- [10] F. De Gaetano, M. Serrani, P. Bagnoli, J. Brubert, J. Stasiak, G. D. Moggridge e M. L. Costantino, «Fluid dynamic characterization of a polymeric heart valve prototype (Poli-Valve) tested under continuous and pulsatile flow conditions,» *International Journal of Artificial Organs*, vol. 38, n. 11, 2015.
- [11] D. J. Kereiakes, G. A. Answini, S. J. Yakubov, B. Rai, J. M. Smith, S. Duff, F. L. Shannon, M. Sakwa, J. Beith e D. Heimansohn, «Preliminary Evaluation of a Novel Polymeric Valve Following Surgical Implantation for Symptomatic Aortic Valve Disease,» *JACC: Cardiovascular Interventions*, vol. 14, n. 24, pp. 2754-2756, 2021.
- [12] S. Y. Ho, «Structure and anatomy of the aortic root,» *European Journal of Echocardiography*, vol. 19, n. 1, 2009.
- [13] R. Toninato, J. Salmon, F. M. Susin, A. Ducci e A. Ducci, «Physiological vortices in the sinuses of Valsalva: An in vitro approach for bio-prosthetic valves,» *Journal of Biomechanics*, vol. 49, n. 13, 2016.
- [14] H. Reul, A. Vahlbruch, M. Giersiepen, T. Schmitz-Rode, V. Hirtz e S. Effert, «The geometry of the aortic root in health, at valve disease and after valve replacement,» *Journal of Biomechanics*, vol. 23, n. 2, 1990.
- [15] R. M. Lang, B. P. Cholley, C. Korcarz, R. H. Marcus e S. G. Shroff, «Measurement of Regional Elastic Properties of the Human Aorta A New Application of Transesophageal Echocardiography With Automated Border Detection and Calibrated».
- [16] Z. Liu, C. T. Ting, S. Zhu e F. C. Yin, «Aortic compliance in human hypertension,» *Hypertension*, vol. 14, n. 2, 1989.
- [17] ViVitro, «Pulse duplicator».
- [18] B. Laboratories, «Test Equipment».
- [19] O. Bazan e J. P. Ortiz, «Experimental validation of a cardiac simulator for in vitro evaluation of prosthetic heart valves,» *Brazilian Journal of Cardiovascular Surgery*, vol. 31, n. 2, pp. 151-157, 2016.
- [20] I. Spee, G. Cacciola, G. Peters e J. Janssen, «In-vitro Testing of Trileaflet Heart Valve Prostheses,» Eindhoven university of technology, 1997.

- [21] A. Armagno, M. L. Costantino, D. Obrist, F. Clavica e L. Pietrasanta, «Design and Manufacturing of a Compliant Aortic Model by means of CAD Modelling and 3D Printing,» 2020.
- [22] C. M. García-Herrera, J. M. Atienza, F. J. Rojo, E. Claes, G. V. Guinea, D. J. Celentano, C. García-Montero e R. L. Burgos, «Mechanical behaviour and rupture of normal and pathological human ascending aortic wall,» *Medical and Biological Engineering and Computing*, vol. 50, n. 6, 2012.
- [23] Formlabs, «Elastic 50A Datasheet».
- [24] «BSI Standards Publication Rubber, vulcanized or thermoplastic-Determination of tensile stress-strain properties,» 2017.
- [25] «Polymer Database,» [Online]. Available: <https://polymerdatabase.com/polymer%20physics/Flory%20Rehner.html>.
- [26] J. W. Stansbury e M. J. Idacavage, «3D printing with polymers: Challenges among expanding options and opportunities,» *Dental Materials*, 2016.
- [27] F. De Gaetano, M. L. Costantino e S. Farè, «Design, manufacturing and in-vitro testing of an innovative biomorphic heart valve made of a new thermoplastic elastomeric biomaterial,» Politecnico di Milano, 2017.
- [28] B. S. Institution, «Cardiovascular implants. Cardiac valve prostheses. Part 1, General requirments.».
- [29] P. Lu, J. Liu, R. Huang, C. Lo, H. Lai e N. Hwang, «The closing behavior of mechanical aortic heart valve prostheses,» *ASAIO Journal*, 2004.
- [30] B. Laboratories, «Test Equipment».

List of Figures

Figure 1.1: The cardiovascular system	3
Figure 1.2: Phases of the cardiac cycle.....	5
Figure 1.3: View of the valve plane with the four valves clearly visible.....	6
Figure 1.4: Anatomy of the aortic valve	6
Figure 1.5: Bileaflet mechanical valve	7
Figure 1.6: Stented biological valve	8
Figure 1.7: Tria heart valve, made with Lifepolymer by Foldax	8
Figure 1.8: Structure of vessel downstream the aortic valve	9
Figure 1.9: Anatomy of the aortic valve	10
Figure 2.1: ViVitro standard set up with compliant accessory	14
Figure 2.2: BDC Labs Pulse Duplicator	15
Figure 2.3: Cardiac simulator.....	15
Figure 2.4: Test bench with vertically moving	16
Figure 2.5: Schematic representation of the pulse duplicator used in this work	17
Figure 2.6: Compliant silicone aortic model.....	18
Figure 3.1: Printer (a) and printing example (b)	20
Figure 3.2: Geometry of uniaxial tensile samples	21
Figure 3.3: Schematic representation of the different orientations.	24
Figure 3.4: Section of the conduit.....	25
Figure 3.5: Experimental set up.....	26
Figure 3.6: Percentage increase for samples during testing.....	29
Figure 3.7: Stress-strain curves obtained from tensile test	31
Figure 3.8: Stress-strain curves for samples printed in different directions	32
Figure 3.9: Printing chamber positioning for isotropy tests.....	33
Figure 3.10: Results of the creep experiment.....	34
Figure 3.11: Results of stress relaxation experiment	35

Figure 3.12: Results of the pressurization tests	36
Figure 3.13: Results of the cyclic experiment at 100%.....	37
Figure 3.14: Stress and strain time behavior at 25% strain	38
Figure 3.15: Cyclic behavior.....	39
Figure 3.16: Hysteresis loops of the 25% strain experiment.....	40
Figure 3.17: E^* and $\text{tg}\delta$ as function of time for 2 samples.....	41
Figure 3.18: E^* and $\text{tg}\delta$ as function of frequency	41
Figure 3.19: Moduli in frequency sweep.....	42
Figure 3.20: E^* and $\text{tg}\delta$ as a function of time, comparison between air and water.....	43
Figure 4.1: Picture of the set up for straight and rigid	46
Figure 4.2: Schematic of measurements of the aortic root.....	47
Figure 4.3: CAD model for rigid conduit with Valsalva sinuses.....	48
Figure 4.4: Picture of set up for rigid with geometry	48
Figure 4.5: CAD model for the compliant conduit	49
Figure 4.6: Picture of set up for compliant with geometry.....	50
Figure 4.7: Picture of the mechanical valve used for tests.....	50
Figure 4.8: Schematic of support for mechanical valve	51
Figure 4.9: Biological valve used for tests.....	51
Figure 4.10: Schematic of support for biological valve	52
Figure 4.11: Polymeric valve used for tests	52
Figure 4.12: Downstream pressure, Upstream pressure and aortic flowrate.....	53
Figure 4.13: Example of calculation of pressure difference.....	53
Figure 4.14: Graph showing flowrate vs time in cycle as given in the Standard.....	54
Figure 4.15: Videos showing the mechanical, polymeric, and biological prostheses..	55
Figure 4.16: Upstream, downstream, and differential pressure	56
Figure 4.17: Pressure difference for the mechanical valve	57
Figure 4.18: Flow for mechanical valve.....	60
Figure 4.19: Flow for polymeric valve.....	60
Figure 4.20: Flow for biological valve.....	61
Figure 4.21: Regurgitation for mechanical valve	62
Figure 4.22: Regurgitation for polymeric valve	62

Figure 4.23: Regurgitation for biological valve 63

Figure 4.24: Upstream pressure for mechanical valve 64

Figure 4.25: Upstream pressure for polymeric valve 65

Figure 4.26: Upstream pressure for biological valve..... 65

Figure 4.27: Downstream pressure for mechanical valve..... 66

Figure 4.28: Downstream pressure for polymeric valve..... 67

Figure 4.29: Downstream pressure for biological valve 67

List of Tables

Table 3.1: Time points of swelling test	21
Table 3.2: Testing conditions for linearity experiment	25
Table 3.3: Testing condition of cyclic DMA tests	27
Table 4.1: Geometric ratios of the aortic root	47
Table 4.2: MPD results for each of the tested conditions	55
Table 4.4: SV results for each of the tested conditions	57
Table 4.3: Q_{RMS} results for each of the tested conditions	58
Table 4.5: EOA results for each of the tested conditions	58
Table 4.6: Requirements for EOA as listed in the Standard	58
Table 4.7: Regurgitation results for each of the tested conditions	59
Table 4.8: Flow behavior in each testing condition for each valve	60
Table 4.10: Regurgitant flow behavior in each testing condition for each valve	62
Table 4.11: Results for closing and leakage volume for each condition	64
Table 4.12: Upstream pressure behavior in each testing condition for each valve	64
Table 4.13: Downstream pressure behavior in each testing condition for each valve	66

List of symbols

Variable	Description	SI unit
σ	Stress	Pa
ε	Strain	/
P	Pressure	Pa or mmHg
r	Internal radius	mm
R	External radius	mm
t	Thickness	mm
ΔA	Area variation	mm ²
E	Young Modulus	Pa
E^*	Complex modulus	Pa
E'	Conservative modulus	Pa
E''	Dissipative modulus	Pa
$tg\delta$	Ratio E''/E'	/
λ	Geometric parameter	/
Q	Flow	L/min
ΔP	Pressure variation	mmHg
ΔV	Volume variation	cm ³

Glossary of Acronyms

<i>TAVI</i>	Transcatheter Aortic Valve Implantation
<i>EPDM</i>	Ethylene-Propylene Diene Monomer
<i>CAD</i>	Computer Aided Design
<i>STL</i>	STero Lithography interface
<i>DMA</i>	Dynamic Mechanical Analysis
<i>MSPD</i>	Mean Systolic Pressure Difference
<i>Q_{RMS}</i>	root mean square of forward flow
<i>EOA</i>	Effective Orifice Area
<i>RG</i>	ReGurgitant volume

Acknowledgments

I would like to thank everyone that supported and helped me during this work; my family, my very patient boyfriend and the teams at LaBS and at the polymers' lab who encouraged me all the way.

